Dear Author,

Please, note that changes made to the HTML content will be added to the article before publication, but are not reflected in this PDF.

Note also that this file should not be used for submitting corrections.

Biochimica et Biophysica Acta xxx (2016) xxx–xxx

Contents lists available at ScienceDirect

Biochimica et Biophysica Acta

journal homepage: www.elsevier.com/locate/bbamcr

Perrin and Förster unified: Dual-laser triple-polarization FRET (3polFRET) for interactions at the Förster-distance and beyond

Tamás Ungvári [b], Péter Gogolák [a], Miklós Bagdány [c], László Damjanovich [d], László Bene [d,*]

[a] Department of Immunology, Faculty of Medicine, University of Debrecen, Debrecen, Hungary
[b] Department of Biophysics and Cell Biology, Faculty of Medicine, University of Debrecen, Debrecen, Hungary
[c] Department of Physiology, McGill University, Montreal, Canada
[d] Department of Surgery, Faculty of Medicine, University of Debrecen, Debrecen, Hungary

ARTICLE INFO

Article history:
Received 18 December 2015
Received in revised form 1 February 2016
Accepted 3 February 2016
Available online xxxx

Keywords:
Triple-anisotropy correlations
Donor anisotropy
Acceptor anisotropy
Orientation factor for FRET
Homo-FRET relief
FRET-fraction

ABSTRACT

Dual laser flow cytometric energy transfer (FCET) – elaborated by Trón et al. in 1984 – is an efficient and rapid way of measuring FRET on large cell populations. FRET efficiency and the donor and acceptor concentrations are determined from one donor and two acceptor signals. In this communication this method is extended towards the domain of receptor dynamics by the detection of polarized components of the three intensities. By enabling a complete description of the proximity and dynamics of FRET-systems, the new measuring scheme allows a more refined description of both the structure and dynamics of cell surface receptor clusters at the nano-scale and beyond. Associated donor fraction, limiting anisotropy and rotational correlation time of the donor, and cell-by-cell estimation of the orientation factor for FRET (κ^2) are available in the steady state on a single FRET sample in a very rapid and statistically efficient way offered by flow cytometry. For a more sensitive detection of conformational changes the "polarized FRET indices" – quantities composed from FRET efficiency and anisotropies – are proposed. The method is illustrated by measurements on a FRET system with changing FRET-fraction and on a two donor-one acceptor-system, when the existence of receptor trimers are proven by the detection of "hetero-FRET induced homo-FRET relief", i.e. the diminishing of homo-FRET between the two donors in the presence of a donor quencher. The method also offers higher sensitivity for assessing conformational changes at the nano-scale, due to its capability for the simultaneous detection of changes of proximity and relative orientations of the FRET donor and acceptor. Although the method has been introduced in the context of FRET, it is more general: It can be used for monitoring triple-anisotropy correlations also in those cases when FRET actually does not occur, e.g. for interactions occuring beyond the Förster-distance R_0. Interpretation of κ^2 has been extended.

1. Introduction

Even in the era of super-resolution microscopy, like stimulated emission depletion (STED) microscopy, FRET remains amongst the leading methodologies for revealing conformations, dynamics and clustering of biological macromolecules on the 1–10 nm distance scale [1–5]. During FRET a portion of the excitation energy of the donor is tunneled to a nearby acceptor having an absorption adequately overlapping with the donor's emission on the wavelength scale, and dipole orientations favorable for FRET [6–9]. FRET is measured by detecting its characteristic effects on the fluorescence properties of the donor and acceptor: decreased fluorescence lifetime leading to decrease of fluorescence intensity (quenching) and decreased photobleaching, and increased fluorescence anisotropy on the donor side, increased emission (sensitized emission) and photobleaching, decreased anisotropy on the acceptor side [1–5].

In the scheme of the conventional "flow cytometric FRET" (FCET) method FRET efficiency and the donor and acceptor concentrations are determined from the simultaneous detection of donor quenching and the sensitized emission of acceptor [9–12]. The latter quantities are determined from one donor intensity (I_1) and the two acceptor intensities (I_2, I_3). Although the FCET method, as it stands, has been applied in the past in many cases successfully for revealing conformational changes and cell surface receptor patterns [13–16], taking into account polarization in its all three detected signals offers new opportunities for detecting fine details of dynamics and structure of receptor clusters. By detecting the polarized components of the three signals three new quantities, the donor anisotropy, the anisotropy of the sensitized emission of acceptor and the anisotropy of the directly excited acceptor are available, all in the

Abbreviations: FRET, fluorescence resonance energy transfer; MHCI/MHCII, Class I/Class II Major Histocompatibility Complex protein; β_2m, beta-2 microglobulin, the light chain (l.c.) component of MHCI; mAb, monoclonal antibody.

* Corresponding author at: Department of Biophysics and Cell Biology, University of Debrecen, H-4012 Debrecen, P.O. Box 39, Hungary.
E-mail address: bene@med.unideb.hu (L. Bene).

http://dx.doi.org/10.1016/j.bbamcr.2016.02.002
0167-4889/

presence of FRET. The pertinent polarization characteristics of FRET behind the observations are the following (Fig. 1): On the donor side, reduction of lifetime by FRET may increase anisotropy, due to the shortage of time available for rotation of the fluorophore [17–21]. For donors completely associated with acceptors – unity FRET-fraction – the analysis of the reciprocal anisotropy-"complement FRET" (1-E) "Perrin-plots" makes possible the determination of the limiting anisotropy and the rotational correlation time [19–21]. These quantities can further be used for the computation of FRET fraction in those cases when the donors are not completely associated with acceptors, i.e. the FRET-fraction is smaller than unity. On the acceptor side, in addition to the directly excited portion of fluorescence, the sensitized emission appears with an anisotropy generally much smaller than that of the directly excited component [21–30]. The reduced anisotropy of sensitized emission is a consequence of the depolarized way of excitation by the curvy field lines of the donor dipole and as such it depends on the orientation and position of the acceptor dipole in the donor dipole field [4,8,9]. In contrast, the anisotropy of the directly excited acceptor fluorescence may depend on steric constraints on acceptor rotation imposed by the donor bearing tags.

In this communication, by the correlated analysis of these anisotropies with FRET in the steady-state, in the spirit of the work of Dale et al. [6] we attempt to give a more refined "global" description of sructure and dynamics of donor-acceptor systems via the deduction of quantities such as FRET-fraction, limiting anisotropy, rotational correlation time and orientation factor for FRET (κ^2), belonging also to the realm of the different time-resolved (FLIM) techniques [26,29,31,32].

Based on the FRET efficiency and the donor anisotropies as primarily measured quantities, new quantities termed polarized FRET-indices have also been defined aiming at a sensitive detection of conformational changes [33]. A flow chart summarizing the main ideas behind the method is presented in Fig. 2.

FRET between identical fluorophores ("homo-FRET") can also lead to an anisotropy reduction, mimicking Brownian-rotation [23,24,30]. An implication is that, in the presence of acceptor, the anisotropy of a homo-FRET-coupled donor system may increase not only via the reduced time available for Brownian-rotation but also by the reduced time available for homo-FRET. In effect homo-FRET may be "quenched" by nearby acceptors in close proximity ("homo-FRET relief"). The working principles of the 3polFRET method are illustrated by a two donors-one acceptor system aiming at the detection of receptor trimers. The physical proximity of the light (β_2m) and heavy chain (h.c.) components of the MHCI molecule and the MHCII molecule – a three component-system – have been proven in the past with different methods. We show with 3polFRET that homo-FRET between labels bound on any two of these elements may efficiently be cut by an acceptor bound to the third element. Also with this system illustrated is the usefulness of the polarized FRET indices introduced for sensitively monitoring conformational changes.

Another field of application of 3polFRET rests on the possibility for the determination of the limiting anisotropies (r_0) of the donor and acceptor and the anisotropy of sensitized emission. The lower and upper limits of the κ^2 orientation factor for FRET and the corresponding lower and upper distance limits are determined on a cell-by-cell basis in the framework of a "Dale–Eisinger style" analysis [6–9,34,35] detailed in the *Supporting information*.

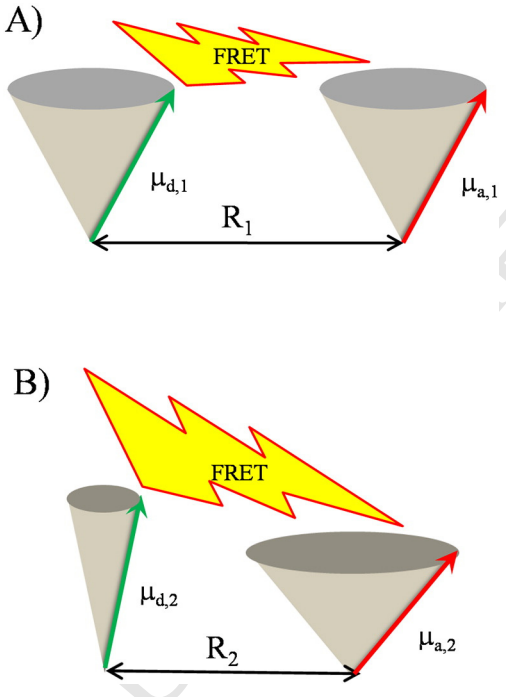

Fig. 1. *Polarization effects of FRET.* Panel A: Shown are, orientation distributions of donor (green cone) and acceptor dipoles (red cone) at large mean separation R_1, with a low level of FRET. Panel B: Orientation distributions of donor and acceptor dipoles at smaller mean separation R_2, with an increased level of FRET. Increased FRET due to shortening of donor-acceptor separation ($R_2 < R_1$) leads to narrowing and broadening of orientation distribution of donor and acceptor excited state dipoles, illustrated by cones with the green and red arrow, respectively. They are shown on the surface of the cones, but could be anywhere in the conical volumes. In parallel, the reduced volume of the cone of donor dipoles reflects reduced intensity and fluorescence lifetime due to the donor quenching — dipoles at larger angles are inclined to be quenched preferably. The increased volume of the cone of acceptor dipoles reflects increased intensity (sensitized emission) due to the indirect excitation by the curvy donor dipole fields — extra dipoles appear at larger angles. The lengths of the individual donor and acceptor dipoles – and consequently, the radiative rates and intrinsic lifetimes – are not affected ($\mu_{d,1} = \mu_{d,2}$, $\mu_{a,1} = \mu_{a,2}$).

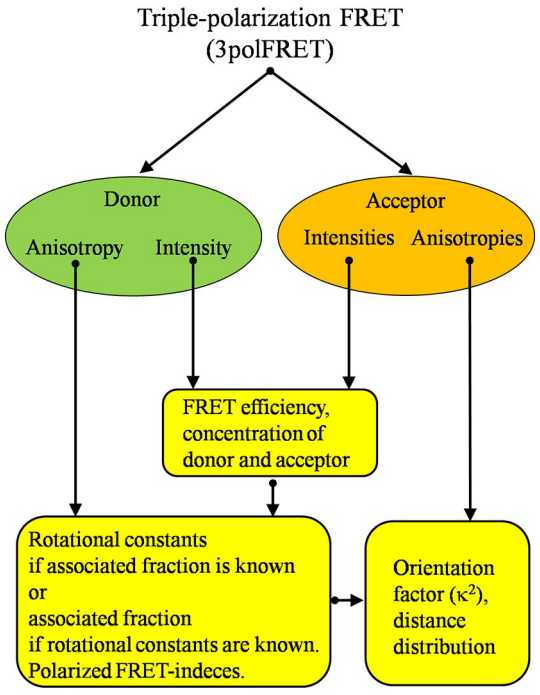

Fig. 2. *Flow-chart of the triple-polarization FRET (3polFRET) method.* The fluorescence anisotropies and intensities of the donor and acceptor are the primarily measured quantities (in the ellipses). The FRET efficiency and the amount of the donor and acceptor are computed from the total intensities of the donor and acceptor (in the rectangles). The donor anisotropy is used either for describing rotational motion of the donor if the associated donor fraction is known, or – as a refinement of the characterization of the receptor clusters – for the computation of the associated donor fraction if the rotational constants of the donor are the known quantities. The polarized FRET indices are defined as combinations of the donor anisotropies and FRET efficiency. The computation of orientation factor and subsequently the distance distributions rests on the knowledge of the rotational constants of both the donor and acceptor.

Please cite this article as: T. Ungvári, et al., Perrin and Förster unified: Dual-laser triple-polarization FRET (3polFRET) for interactions at the Förster-distance and beyond, Biochim. Biophys. Acta (2016), http://dx.doi.org/10.1016/j.bbamcr.2016.02.002

2. Materials and methods

2.1. Cell line

The JY B cell line was originally described in [36]. Cells were cultured in RPMI-1640 medium supplemented with 10% fetal calf serum, penicillin and streptomycin [36].

2.2. Monoclonal antibodies

The production and specificity of monoclonal antibodies (mAbs) applied in the experimental procedures have been described earlier [13,34]. MAbs W6/32 ($IgG_{2a\kappa}$) and L368 ($IgG_{1\kappa}$) developed against a monomorphic epitope on the α_2, α_3 domains of the heavy chain and the β_2-microglobulin of MHCI, respectively [13,34,35]; mAb L243 ($IgG_{2a\kappa}$) against MHCII, DRα were kindly provided by Dr. Frances Brodsky (UCSF, CA). These mAbs were prepared from supernatants of hybridomas and were purified by affinity chromatography on protein A-Sepharose.

2.3. Fluorescent staining of antibodies

Aliquots of the proteins for fluorescence conjugation were labeled with 6-(fluorescein-5-carboxamido)hexanoic acid, succinimidyl ester (xFITC) (Molecular Probes, Eugene, OR) or Alexa-Fluor 488 (A488) as the donor dyes, and Alexa-Fluor 546 (A546) as the acceptor dye (Invitrogen). xFITC has a large amplitude tethered motion (segmental mobility) because it contains a 7-atom aminohexanoyl spacer ("x") between the fluorophore and succinimidyl ester moieties. Kits provided with the dyes were used for the conjugation. Detailed labeling procedure of the mAb was described earlier [13,39,40]. Dye-per-protein labeling ratios for the A488-(A546-)conjugated L243, L368, and W6/32 mAbs were 2.4 (2.14), 3.16 (2.8), and 1.8 (1.8), respectively. Labeling ratios for xFITC-conjugated L368 and W6/32 mAbs were 3.9 and 3.7, respectively. These values were separately determined for each labeled aliquot in a spectrophotometer (Hitachi U-2900, NanoDrop ND-1000) [13]. The labeled proteins retained their affinity as proven by competition experiments with identical, unlabeled ligands.

2.4. Labeling of cells with mAbs

Freshly harvested cells were washed twice in ice cold PBS (pH 7.4), the cell pellet was suspended in 100 μl of PBS (10^6 cells/ml) and labeled by incubation with ~10 μg of dye-conjugated mAbs for 40 min on ice in the dark. The excess of mAbs was at least 30-fold above the K_d during incubation. To avoid possible aggregation of the dye-conjugated mAbs, they were air-fuged (at 110,000 g, for 30 min) before labeling. Special care was taken to keep the cells at ice cold temperature before FRET measurements in order to avoid unwanted aggregations of cell surface receptors or receptor internalization. Labeled cells were washed twice with ice cold PBS and then fixed with 1% paraformaldehyde. The single acceptor-labeled and the double-labeled (with both donor and acceptor) samples were titrated according to the surface concentration of the acceptor carrying mAb. In these samples the cells were treated identically, except for the amount of acceptor-stained antibodies used for labeling: it has been gradually increased until the final saturating concentration was achieved. The final concentrations in the titration series in μM for mAbs L368 and W6/32 were 0.734 and 0.686, respectively.

2.5. Flow cytometric triple-anisotropy measurements

Cell-by-cell basis correlated measurements of the polarized intensity components – from which the total intensities and anisotropies are calculated – of the donor and acceptor were carried out in a „triple T-format" arrangement [19,24,41–43] (Fig. 3). It was realized in a Becton–Dickinson flow cytometer (FACSVantage SE with a FACSDiVa extension) equipped with dual-laser excitation, with the lasers operating in the single line mode at 488 nm (Coherent Enterprise Ar^+-ion gas laser, Innova Technology) and at 532 nm (a diode-pumped solid-state laser), by placing three broadband polarization beam splitter cubes (10FC16PB.3, Newport) in the donor and two acceptor fluorescence channels. The fluorescence intensities of the green (xFITC, Alexa-Fluor 488) donor dyes and the red acceptor dyes (xTRITC, Alexa-Fluor 546) were excited at the 488-nm and the 532-nm laser lines and were detected orthogonally to the direction of the exciting laser light beams by green and red sensitive photomultiplier tubes (side on, Hamamatsu). Signals I_1 and I_2 both activated by the blue laser line at 488 nm were separated by a dichroic mirror (580 nm), then transmitted through a 535 ± 15 nm- and a 640 ± 60 nm-band pass filter (HQ535/30, HQ 640/120, AF Analysentechnik, Tübingen) before reaching the polarization crystals which split them into their vertical and horizontal components. Signals I_{1h}, I_{1v} are detected at the flow cytometer photomultiplyer ports FL_1 and FL_2, and I_{2h}, I_{2v} at FL_3 and FL_7. Signal I_3 activated by the green laser line at 532 nm is projected by a silvered metal mirror through a 640 ± 60 nm-band pass filter (HQ 640/120) on the 3rd beam splitter cube which splits it into the I_{3h} and I_{3v} components detected at the FL_4 and FL_5 photomultiplyer ports. For the determination of the G-factor of each fluorescence channel, the originally vertical polarization direction of laser light is rotated by 90° with zero order quartz wave plates (half-wave retarders HWR_1: 10RP02–12 for 488 nm, and HWR_2: 10RP02–16 for 532 nm, Newport) positioned between the lasers and the cytometer via micro rotary stages (M-481-A, Newport). The orientations of the half-wave retarders have been calibrated in advance by recording the dependence of the polarized fluorescence intensities of fluorescent microbeads on the angle of the retarders.

2.6. Calculation of total intensities and anisotropies

Four polarized intensities have been detected for each signal channel [21,24,30]: $I_{i,vv}$, $I_{i,vh}$, $I_{i,hv}$, and $I_{i,hh}$, with the first index *i* designating the signal channel, the second and third ones referring to the polarization direction of the exciting laser light and that of the fluorescence, respectively. The signals with the horizontal excitation are detected after the vertical excitation by rotating the polarization direction with 90°. After subtracting the corresponding background intensities measured on the unlabeled cells from the polarized intensities, the correction factors G_i (i = 1–3) balancing the sensitivities of vertical and horizontal fluorescence channels, the total fluorescence intensities I_i, and the fluorescence anisotropies r_i were calculated as follows:

$$G_i = {}^{I_{i,hv}}\!/_{I_{i,hh},} \quad (1)$$

$$I_i = I_{i,vv} + \hat{a}(\psi) \cdot G_i \cdot I_{i,vh}, \quad (2)$$

$$r_i = {}^{(I_{i,vv} - G_i \cdot I_{i,vh})}\!/_{I_{i.}} \quad (3)$$

In the above expression for the total intensities I_i (i = 1–3) a numerical correction for the high aperture fluorescence collection was carried out according to T. M. Jovin [24,43] by using the term $\hat{a}(\psi) = 1 + \cos\psi \cdot (1 + \cos\psi)/2$, where $\hat{a}(\psi)$ assumes a value of 1.72 for our numerical aperture of NA = 0.6, and ψ stands for the half angle of the detected light cone. The anisotropy and total intensity values were computed on a cell-by-cell basis from the correlated $I_{i,vv}$ and $I_{i,vh}$ intensities with predetermined values of the G_i factors as input parameters. Based on Eq. (2) the r_{corr} aperture-corrected anisotropy can be written as the function of the r uncorrected one as follows:

$$r_{corr} = 3 \cdot r / \{1 + \hat{a}(\psi) + r \cdot [2 - \hat{a}(\psi)]\}. \quad (4)$$

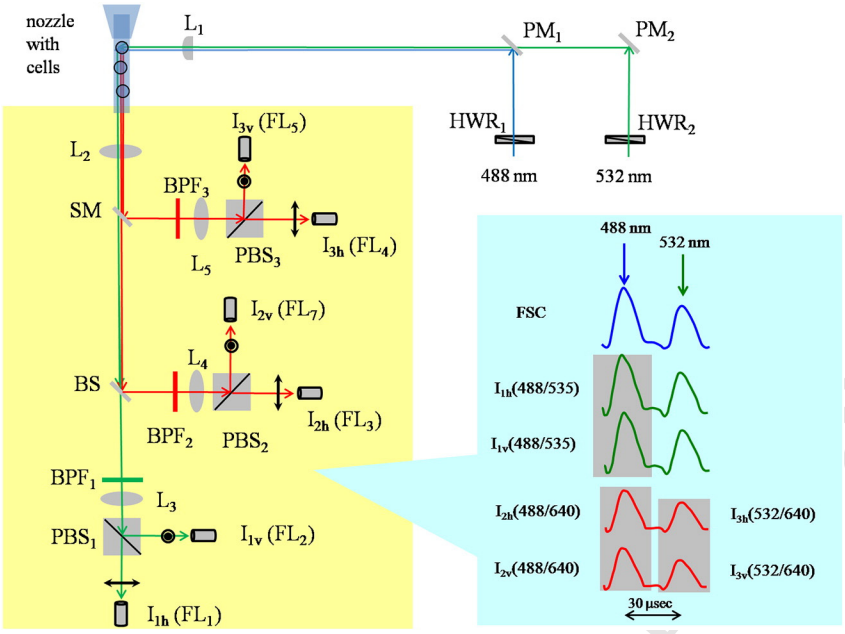

Fig. 3. *Scheme of "triple T-format" optical arrangement for the combined measurement of the donor and acceptor anisotropies: top view of triple-polarization FRET (3polFRET) with the collected signals.* The cells are illuminated through the main focusing lens L_1, by the blue and green laser lights whose polarization direction can be adjusted by the HWR_1 and HWR_2 half-wave retarders. The fluorescence intensities of the donor and acceptor (green, red) are collected by the lens L_2 (NA = 0.6). The fluorescence intensities activated by the blue laser are dispersed by dichroic beam splitter BS (580 nm) into green and red components (I_1, I_2), which are projected through band pass filters BPF_1 (535 ± 15 nm), BPF_2 (640 ± 60 nm) and relay lenses L_3, L_4 onto the polarization beam splitter cubes PBS_1, PBS_2. The fluorescence activated by the green laser (I_3) is projected by the silvered mirror SM on the polarization beam splitter cube PBS_3 through the band pass filter BPF_3 (640 ± 60 nm) and relay lens L_5. The polarization direction of the illuminating laser light beams can be rotated into the perpendicular direction for the measurement of the G-factors by the HWR_1 and HWR_2 half-wave retarders. The polarization direction in the plane of the drawing (horizontal) is represented by double-ended arrows, the perpendicular polarization (vertical) by encircled dots. PM_1, PM_3 right angle prisms for mirroring light from the lasers into the cytometer's ports. FSC: forward (small angle) light scattering, I_1: donor intensity, I_2: sensitized acceptor intensity, I_3: directly excited acceptor intensity. There is ~30 μs lag between the signals activated by the two laser lines.

The significance of this formula is that it can be used also in the reverse direction: the unknown $\hat{a}(\psi)$ aperture term can be computed from the measured value of r in the knowledge of the anisotropy r_{corr} of a calibrated standard.

The mean values of fluorescence anisotropy and total intensity histograms measured on the single donor- or acceptor-labeled cells (for ~10^4 cells) were further used for the calculation of the necessary input constants α, S_1, S_2, and S_3 for constructing the histograms of the most important resulting quantities of the 3polFRET method: E, I_d, I_a, r_1, r_{et} and r_a. The average values of the means of anisotropy histograms obtained in different measurements with their standard errors were also determined and tabulated. The generation and subsequent analysis of flow cytometric histograms (like the ones on Fig. 4) and 2-D correlation plots (dot-plots) of total fluorescence intensities, fluorescence anisotropy, and FRET efficiency were performed by a home-made software specialized for flow cytometric data analyses called Reflex, written by G. Szentesi [44], freely downloadable from http://www.biophys.dote.hu/research.htm, and http://www.freewebs.com/cytoflex.htm, or from the corresponding author bene@med.unideb.hu.

3. Theoretical results

3.1. Theory of triple-polarization FRET (3polFRET)

3.1.1. Anisotropy of sensitized and directly excited emission of acceptor

Our starting point is the knowledge of the total intensities I_1, I_2, I_3 and the corresponding fluorescence anisotropies r_1, r_2, r_3 measured at the excitation wavelength of the donor (channels 1, 2) and of the acceptor (channel 3) [10–12,19]. The definitions and way of measuring these quantities in terms of polarized intensity components are described in the *Materials and methods*. From the total intensities I_1, I_2, I_3, the FRET efficiency E, and the donor and acceptor intensities I_d, and I_a reflecting the donor and acceptor concentrations of the double-labeled cell sample are determined via the standard method of FCET outlined in the Supplement. In the next we only describe, how the anisotropy of sensitized emission (r_{et}) and the directly excited acceptor emission (r_a) are determined from the r_1, r_2, and r_3 primary anisotropies. We set out by first defining the acceptor intensities and corresponding anisotropies measured in the presence of donor at the donor's and acceptor's excitation wavelength in the acceptor channels, I_{2a}, r_{2a} and I_{3a}, r_{3a} [41,42]:

$$I_{2a} \equiv I_a \cdot S_2 + I_1 \cdot A, \tag{5}$$

$$I_{3a} \equiv I_a + I_1 \cdot A' \cdot S_3/S_1, \tag{6}$$

$$r_{2a} \equiv \left(I_a \cdot S_2 \cdot \rho_2 \cdot r_a + I_1 \cdot A' \cdot r_{et}\right)/I_{2a}, \tag{7}$$

$$r_{3a} \equiv \left[I_a \cdot r_a + I_1 \cdot A' \cdot (r_{et}/\rho_2) \cdot S_3/S_1\right]/I_{3a}, \tag{8}$$

with the A′ helper quantity and ρ_2 anisotropy conversion factor defined in Eqs. 4 s, 17 s of the *Supporting information*. The first terms of the I_{2a} and I_{3a} intensities containing I_a correspond to the directly excited, the second ones containing A′, the indirectly excited intensity components. According to Eqs. (7) and (8), both r_{2a} and r_{3a} are smaller than r_a, because these parameters are weighted averages of r_a and r_{et}, and the latter is generally much smaller than r_a. By inspecting the expanded forms of I_2, and I_3 in the Supplement, alternative forms of I_{2a} and I_{3a} can be found as

$$I_{2a} = I_2 - I_1 \cdot S_1, \tag{9}$$

$$I_{3a} = I_3 - I_1 \cdot S_3. \tag{10}$$

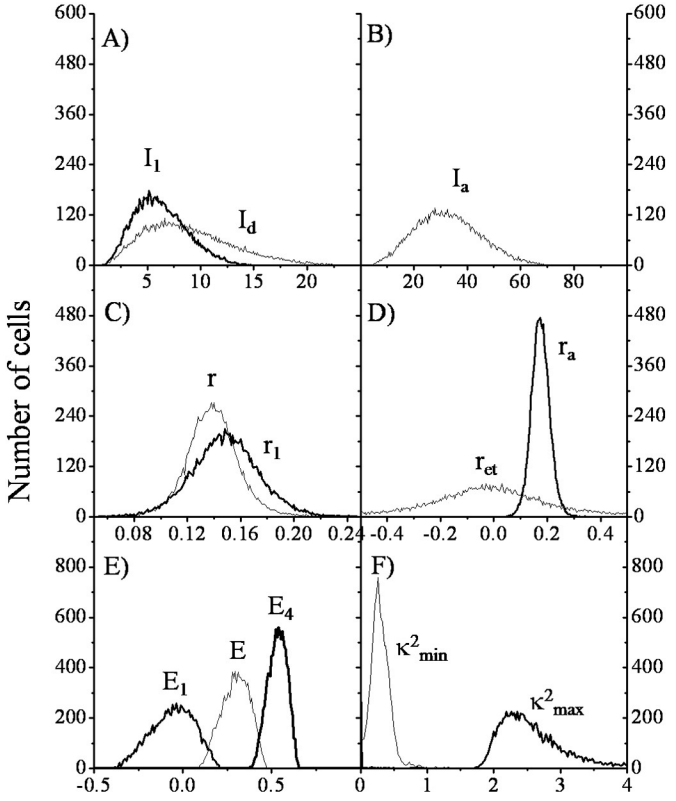

Fig. 4. *Characteristic flow cytometric distributions of the 3polFRET method.* The unquenched donor intensity I_d, the directly excited acceptor intensity I_a, and the FRET efficiency distribution E are computed from the total I_1, I_2 and I_3 intensities in the conventional manner by using the S_1, S_2, S_3 and α spectroscopic-optical constants. The relative magnitude of I_1 as compared to I_d (thick and thin lines on Panel A) is reduced in proportion with the FRET efficiency E due to the quenching by FRET. The I_a (Panel B) and I_d intensities are the input parameters for determining the acceptor-donor concentration ratios and the f_0 FRET fractions in Table 1. In Panel C the donor anisotropy in the presence of acceptor r_1 is shown together with the anisotropy r of the donor-only sample. As compared to r, anisotropy r_1 is shifted to the right due to FRET. One of the two parameters, the associated donor fraction f and the limiting anisotropy r_0 of the donor can be determined in the knowledge of the other parameter, and r, r_1 and E according to the Perrin-equation extended for partial donor associations. On Panel D: r_a (thin line) is the anisotropy of the directly excited acceptor and $r_{et.}$ (thick line) is the anisotropy of acceptor excited by FRET. According to the expectation, $r_{et.}$ is distributed around zero. Deviation of r_a, measured in the double-labeled FRET-sample, and the corresponding anisotropy of the I_3 intensity for the acceptor-only sample (r_{3a}) is an indicator of possible steric interaction between the donor and acceptor-carrying ligands. On Panel E, only two of the polarization FRET indices, E_1 (leftmost, thin line) and E_4 (rightmost, thick line), having the largest deviations from E are shown, together with E (middle line). These quantities are defined by mixing of the FRET efficiency E and the donor anisotropies r_1, and r. On Panel F, the lower and upper bounds (thick and thin lines) for the FRET orientation factor κ^2 are displayed. These quantities are computed from the limiting anisotropies for the directly excited donor and acceptor, as well as for acceptor excited by FRET. The histograms have been collected from cells labeled with donor-conjugated L368 and acceptor-conjugated W6/32, both at saturation, against the light and heavy chains of MHCI, the 4th sample of Table 1, Part A. Related reciprocal donor anisotropy vs. "complement FRET efficiency" (1-E), and acceptor anisotropy vs. the FRET-related quantity x_{2a} 2-D correlation plots collected on the MHCI-MHCII system are displayed on Fig. 2s in *Supporting information*.

Based on these and the defining equations for r_2 and r_3 (Eqs. 12s, 13s in Supporting information) a 2nd form of r_{2a} and r_{3a} directly amenable for a cell-by-cell determination, can be isolated from r_2 and r_3:

$$r_{2a} = (I_2 \cdot r_2 - I_1 \cdot S_1 \cdot \rho_1 \cdot r_1)/I_{2a}, \tag{11}$$

$$r_{3a} = (I_3 \cdot r_3 - I_1 \cdot S_3 \cdot \rho_3 \cdot r_1)/I_{3a}. \tag{12}$$

Because in contrast to Eqs. (7), (8) all parameters of Eqs. (11) and (12) are primarily measured known ones, these are the forms of r_{2a} and r_{3a} from which they can be determined on a cell-by-cell basis. After determining r_{2a} and r_{3a}, Eqs. (7) and (8) can be taken as indirect definitions of $r_{et.}$ and r_a, and constitute a system of equations for these two unknowns, with the following solutions:

$$r_{et} = (I_{2a} \cdot r_{2a} - I_{3a} \cdot S_2 \cdot \rho_2 \cdot r_{3a})/[I_1 \cdot A' \cdot (1 - S_2 \cdot S_3/S_1)], \tag{13}$$

$$r_a = [I_{3a} \cdot r_{3a} - I_{2a} \cdot r_{2a} \cdot S_3/(S_1 \cdot \rho_2)]/[I_a \cdot (1 - S_2 \cdot S_3/S_1)]. \tag{14}$$

Based on Eqs. (13), (14), cell-by-cell distribution of $r_{et.}$ and r_a can be determined which can further be used e.g. for the determination of the κ^2 orientation factor (see in *Supporting information*). The value of r_a as compared to the r_3 value of the single acceptor-labeled sample, can shed light on possible steric interaction of the donor-label constraining rotation of the acceptor.

3.1.2. Donor Perrin-plots

An important field of application of the measured r_1, $r_{et.}$ and r_a anisotropies is describing rotational characteristics of the donor and acceptor fluorophores which can reflect dynamics and morphological changes – e.g. through homo-FRET – of receptor clusters. Because the donor anisotropy r_1 contains no overspill contamination, it can directly be used for: (i) the deduction of the rotational constants – the r_0 limiting anisotropy and the ϕ rotational correlation time – of the Perrin-model of an isotropic rotator [21,26,41,42], if the fraction of donors associated with acceptors is unity. For an extension on the hindered rotator please see *Discussion*. (ii) For the deduction of the associated fraction of donors (f) in the knowledge of the rotational constants e.g. after a "calibration" process of the (i) step. For the general model valid for arbitrary associated fraction f, the r_1 anisotropy can be written as the weighted average on donor populations with acceptor and without acceptor (the 1st and 2nd terms in the numerator, respectively):

$$r_1 = [(1 - E_0) \cdot f \cdot r' + (1 - f) \cdot r]/[(1 - E_0) \cdot f + 1 - f], \tag{15}$$

where E_0, and r′ denote the FRET efficiency and anisotropy in the clustered donor population and r the anisotropy in the unclustered one. In this formula both r′ and r can be traced back to the r_0 and ϕ rotational constants by applying the Perrin-equation in the absence and presence of acceptor:

$$r = r_0/(1 + \sigma), \tag{16}$$

$$r' = r_0/[1 + \sigma \cdot (1 - E_0)], \tag{17}$$

with σ denoting the ratio of the τ donor lifetime (unperturbed by FRET) and ϕ,

$$\sigma = \tau/\phi, \tag{18}$$

and the factor 1-E_0 representing the reduction in lifetime due to FRET. In Eq. (16), the anisotropy r can be determined on the donor-only sample. Another formula can be written, by noticing that the primarily measured FRET efficiency E is also a weighted average on the clustered and unclustered donor fractions possessing E_0 and zero FRET efficiencies, i.e. $E = [f \cdot E_0 + (1-f) \cdot 0]/[f + (1-f)]$, leading to:

$$E = f \cdot E_0. \tag{19}$$

Eqs. (15)–(17) and (19) constitute a system of 4 equations for the 5 unknowns: r′, r_0, σ, f and E_0, implying that one of the parameters should be known for the unique solution of the receptor association problem. E.g. they can be solved for f and E_0 when the rotational constants are known, and *vice versa*. In both cases, the final solutions can be expressed in terms of the apparent rotational constant σ_{app} introduced as:

$$\sigma_{app} \equiv (r_1 - r)/[r - r_1 \cdot (1 - E)], \tag{20}$$

which should coincide with the real σ for unit associated fraction. This can be proven with Eqs. (15)–(17), (19) after plugging unity into them for f.

In the knowledge of r_0, first the solution for E_0 in terms of σ_{app} and σ is found by plugging r, r′ and E in Eqs. (16), (17) and (19) into Eq. (15):

$$E_0 = 1-(1-E)\cdot\sigma_{app}/\sigma \ . \tag{21}$$

For using this equation σ_{app} is computed according to Eq. (20), and σ according to the formula for the donor anisotropy in the absence of acceptor, Eq. (16). Then by plugging this expression for E_0 into into Eq. (19) f can be expressed as:

$$f = E/\left[1-(1-E)\cdot\sigma_{app}/\sigma\right] \ . \tag{22}$$

In the reversed direction, when the associated fraction f is the known parameter, first the rotation constant σ can be expressed from Eq. (22) in terms of σ_{app} and f as follows:

$$\sigma = f\cdot(1-E)\cdot\sigma_{app}/(f-E) \ . \tag{23}$$

The consistency of the formalism can be noticed here with Eq. (23), because for equal rotational constants ($\sigma = \sigma_{app}$) the associated donor fraction (f) is unity, and vice versa, as expected. Then limiting anisotropy r_0 can be computed by plugging Eq. (23) for σ into Eq. (16):

$$r_0 = r\cdot\left[1+f\cdot(1-E)\cdot\sigma_{app}/(f-E)\right] \ . \tag{24}$$

For a better illumination of the consistency, in the reversed approach, when the associated fraction (f) is known, both r_0 and σ can be expressed in terms of σ_{app} and f in the following alternative forms:

$$r_0 = r\cdot\left(1+\sigma_{app}\right)\cdot\left(1+\delta_f\right), \tag{25}$$

$$\sigma = \sigma_{app}+\delta_f\cdot\left(1+\sigma_{app}\right). \tag{26}$$

Here δ_f is an f-dependent "perturbation factor" responsible for the deviation of the rotational constants σ and σ_{app} due to an associated fraction smaller than unity, defined as:

$$\delta_f \equiv (1-f)\cdot(1-r/r_1)/(f-E). \tag{27}$$

Eqs. (25)–(27) reveal that, partial associations of donors with acceptors reduce the value of both apparent rotational constants as compared to the real ones, with the amount of reduction proportional to 1 − f:

$$\sigma_{app}-\sigma = -\delta_f\cdot\left(1+\sigma_{app}\right) \ . \tag{28}$$

It can also be seen that the δ_f "perturbation" disappears whenever f is unity leading to a coincidence of σ and σ_{app}.

The rotational constants obtained by assuming a known f value, can further be used e.g. for deducing the depolarization factors, the input parameters of the orientation factor (κ^2), see in *Supporting information*. An example for a donor Perrin-plot displayed in the form a 2-D scatter plot of a FRET-sample is shown on Fig. 2s Panel A in *Supporting information*. Extension of the computation of associated fraction for a hindered rotator is analyzed in the *Discussion*.

3.1.3. Acceptor Perrin-plots

Anisotropy vs. FRET efficiency-related parameters, designated by x_2 and x_3, correlation plots (Perrin-plot-like) can also be constructed on the acceptor side. After plugging I_{2a} and I_{3a} (Eqs. (5), (6)) into Eqs. (13), (14) for $r_{et.}$ and r_a, r_{2a} and r_{3a} can be expressed as functions of x_2 and x_3, with $r_{et.}$ and r_a in them as fitting parameters:

$$r_{2a} = r_{et}+(\rho_2\cdot r_a - r_{et})\cdot x_{2a}, \tag{29}$$

with

$$x_{2a} \equiv 1/\left[1+\left(I_1\cdot A'\right)/(I_a\cdot S_2)\right], \tag{30}$$

and

$$r_{3a} = r_{et}/\rho_2+(r_a - r_{et}/\rho_2)\cdot x_{3a}, \tag{31}$$

with

$$x_{3a} \equiv 1/\left[1+\left(I_1\cdot A'\right)\cdot S_3/(I_a\cdot S_1)\right]. \tag{32}$$

By plotting the r_{2a} vs. x_{2a} and similarly r_{3a} vs. x_{3a} scatter plots and fitting them with straight lines, estimations of the mean values of $r_{et.}$ and r_a can be obtained from the intersections and slopes of the fitting lines. In practice the r_{2a} vs. x_{2a} plot gives better results than the r_{3a} vs. x_{3a} plot, because the dependence of x_{3a} on the FRET parameter A′ is weaker than that of x_{2a}, due to the small value of S_3. The parameter A′ is connected with the FRET efficiency E via $I_1\cdot A' = I_d\cdot E\cdot\alpha$, obtainable from Eqs. 5s, 6s in *Supporting information*.

$r_{et.}$ and r_a do not depend on the calibration constant α, in spite of this relation, because A′, I_1, and I_a in Eqs. (29)–(32) are all independent of α. An example for an acceptor Perrin-plot displayed in the form a scatter plot of a FRET-sample is shown on Fig. 2s Panel B in *Supporting information*.

3.1.4. Polarized FRET-indices

For the elaboration of the 3polFRET methodology an impetus was a seek for a method for the sensitive detection of conformational changes and/or rearrangements of elements of cell surface receptor clusters. In this respect, 3polFRET can also be taken as the optical correspondent of the classical mechanical Chasles' theorem [45] (see also Fig. 5), which states that the general motion of a body can always be decomposed to the sum of a rotation and a translation. According to this scheme, FRET efficiency describes mainly translation (notwithstanding now its indirect dependence on rotation through κ^2), and the r_1, $r_{et.}$, and r_a anisotropies mainly the rotation (now notwithstanding dependence of r_1 on E). However, new parameters, called polarized FRET indices, can also be introduced in which FRET efficiency E and the anisotropies combine directly. These parameters are defined by calculating FRET efficiencies

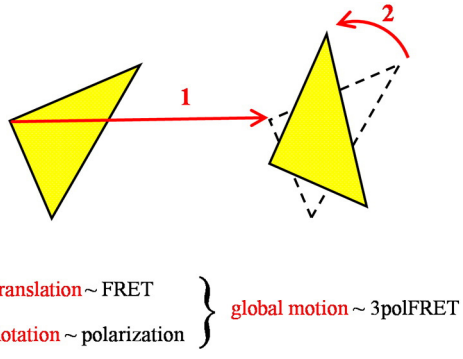

Fig. 5. *Cartoon illustrating the analogy between 3polFRET and the Chasles-theorem of classical mechanics* According to the Chasles-theorem the general motion of a rigid-body represented by the triangle – as a model for a subunit of a biological molecule in a conformational change – can be decomposed to the sum of a translation (1) and a rotation (2). In fluorescence spectroscopy these motional freedoms can be described by measuring FRET and the donor and acceptor anisotropies, respectively. The polarized FRET-indices introduced by Eqs. (32)–(35) for describing conformational changes are combinations of FRET efficiency and donor anisotropies, in which the effects of changing proximity (translation) and orientation (rotation) are measured additively.

Please cite this article as: T. Ungvári, et al., Perrin and Förster unified: Dual-laser triple-polarization FRET (3polFRET) for interactions at the Förster-distance and beyond, Biochim. Biophys. Acta (2016), http://dx.doi.org/10.1016/j.bbamcr.2016.02.002

from the polarized intensity components, instead of the total intensities. For simplicity, considering only the simple donor quenching, the following indices can be defined:

$$E_1(v,h) \equiv 1-I'_{vv}/I_{vh}, \tag{33}$$

$$E_2(v,v) \equiv 1-I'_{vv}/I_{vv}, \tag{34}$$

$$E_3(h,h) \equiv 1-I'_{vh}/I_{vh}, \tag{35}$$

$$E_4(h,v) \equiv 1-I'_{vh}/I_{vv}. \tag{36}$$

Unprimed and primed intensities designate the absence and presence of acceptor, 1st and 2nd subscripts the polarization direction of excitation and emission, respectively. For interpretation of these indices, rotation can be thought of as a special FRET process – after G. Weber [33] – placing photon energy in different orientation states (polarization directions). In this respect, E_1 is the efficiency of FRET which in addition to placing excitation energy to the acceptor side, brings the emitted photon orientation from the horizontal into the vertical position. By using the $I_{vv} = I_{tot}\cdot(1+2\cdot r)/3$ and$I_{vh} = I_{tot}\cdot(1-r)/3$relations (and similarly for the primed intensities), Eqs. (33)–(36) can be cast in the forms showing the explicit dependence on E, r, and r′:

$$E_1(v,h) = 1-(1-E)\cdot(1+2\cdot r')/(1-r), \tag{37}$$

$$E_2(v,v) = 1-(1-E)\cdot(1+2\cdot r')/(1+2\cdot r), \tag{38}$$

$$E_3(h,h) = 1-(1-E)\cdot(1-r')/(1-r), \tag{39}$$

$$E_4(h,v) = 1-(1-E)\cdot(1-r')/(1+2\cdot r). \tag{40}$$

Taking Eqs. (37)–(40) as definitions, cell-by-cell distributions of E_1–E_4 can be calculated from those of E and r′. These quantities may expand (E_1, E_2) or compress (E_3, E_4) the scale of E depending on the r, r′ anisotropies, or equivalently on the r_0 and σ rotational constants. Because E_1 has the largest effect, it seems to be applicable for a sensitive indicator of conformational changes. A detailed analysis of the polFRET indices is presented in the *Supporting information*.

3.2. Experimental results

In the framework of the conventional FCET method, FRET efficiency (E) and quantities proportional to the donor and acceptor levels (I_d, I_a) can be determined in highly efficient manner in a cell-by-cell basis enabling discrimination between subpopulation of cells. Despite the numerous fruitful applications of the FCET method it still have its own caveats and features to be improved, mainly in the following 3 areas: (i) Due to the inherently steady state nature of the method, these data in themselves are average values, offering no insight into the fine structural details of the associations, such as the associated fraction of the donor [31]. (ii) The FRET efficiency besides the donor-acceptor separation depends also on the relative angles of the chromophore dipoles formulated in the orientation factor for FRET κ^2, a quantity on which no information is supplied by the FCET method. As to κ^2, the central question is the error in proximity determination committed by the hypothesis of either the static or the dynamic random limit ($\kappa^2_{static} = 0.476$ and $\kappa^2_{dynamic} = 2/3$) [3,6–9]. (iii) A conformational change in general can be decomposed to the sum a translation and a rotation – in the sense of the classical mechanical Chasles' theorem (Fig. 5) [45] – from which FRET efficiency depends mainly on translation, and with a smaller degree on rotation (notwithstanding now its indirect dependence through κ^2). Is there an optical quantity which directly takes into account both of these motional freedoms? A question, put in the hope of finding a sensitive indicator of conformational changes. For answering these questions, fluorescence anisotropy measurable in the steady state conditions of multiparametric flow cytometry relatively easily and cheaply, is the candidate. Considering the potential FRET dependence of the donor anisotropy via the lifetime involved in the Perrin-equation – traditionally formulated in terms of "quenching resolved anisotropy" (QREA) [3,17] – combining anisotropy and FCET conveys the opportunity to shift the capabilities of the steady state FCET method in the direction of the different time resolved techniques. These are realized mostly in the rather sophisticated and expensive FLIM (anisotropy FLIM, rFLIM) platforms [26,29,31]. For realizing combined measurements of FRET and anisotropy, an advantageous platform is offered by flow cytometry based on its high degree of multiplexing capability and its capability for monitoring large cell populations in a short time, the high throughput nature.

In the next we show that FCET performed in the anisotropy measuring formats of the 3 signal channels (called 3polFRET) is capable for the extension of the conventional FCET to detect rotational motion, associated donor fraction, orientation factor, and to construct new parameters by combining FRET efficiency and donor anisotropy – called "polarization FRET-indices" – some of which may have more sensitivity on conformational changes than FRET and anisotropy separately. An overview of the chief quantities of 3polFRET is presented in Figs. 2, 4.

3.2.1. Determination of rotation constants (r_0, σ) and associated fraction (f) of the donor

Table 1 contains data on a FRET system comprised of donor- and acceptor-labeled mAbs against the light and heavy chains of the MHCI cell surface receptor, with the two subunits representing a system of 1:1 stoichiometry and a well defined intermolecular separation [16]. In Part A, FRET from the L368 (bound to the β_2m) towards the W6/32 (bound to the heavy chain of MHCI), in Part B, FRET in the reversed direction – from W6/32 to L368 – are considered. To reveal the FRET-dependence of the data, the amount of the acceptor, and consequently the magnitude of FRET have been adjusted by changing the amount of the added acceptor-stained mAbs during cell labeling. The primary input data of the Perrin-formalism are the FRET efficiency E, the anisotropies r, r_1 measured on samples labeled only with donor, and both donor and acceptor (Fig. 4, Panel C), and the f_0 associated fraction. The f_0 has been determined at each acceptor concentration by using the computed FCET parameters I_d, I_a and the definition of α (Eqs. 6s, 7s, 11s in *Supporting information*). Essentially two approaches have been followed in the data analysis: (i) in the "forward" approach r_0 has been computed from the measured values of E, r and r_1 at each associated fraction f_0 by using Eqs. (25)–(27). (ii) In the "backward" approach, $r_{1,calc}$ and f have been computed with Eqs. (15), (22) with r_0 and σ determined in the previous "forward" direction at $f_0 = 1$ associated fraction. Considering r donor anisotropies, which are determined partly by rotational mobility of the antibody tethered-dye and partly by homo-FRET – depending on the labeling ratio [19,21,24] – the little larger value of r in the case of L368 (Part A) reports on a more constrained rotation of the dye on this mAb as compared to the W6/32 mAb (Part B).

By inspecting E and r_1 in Part A, both of these parameters monotonously increase with increasing amount of acceptor, as expected. Inspecting now the $r_{1,calc}$ and f quantities recovered by the Perrin-formalism, we can see that while $r_{1,calc}$ excellently follows the experimental r_1 at each f_0 and E, f follows f_0 with small error only after reaching a high enough value of FRET efficiency, in this case ~20%. Accordingly, when the r_0 values are examined, recovering r_0 also fails below the ~20% FRET limit, being these values substantially smaller than the expected r_0 belonging to saturation ($f_0 = 1$). These data imply that high FRET efficiency is the requirement for recovering small associated fractions at a given r_0, or alternatively, for recovering r_0 at a given associated fraction. Similar conclusions can be drawn from data of Part B: Perfect agreement between $r_{1,calc}$ and the experimental r_1 at all f_0, and a tendency for under-estimation of f and r_0. However, the under-estimation is more pronounced, the FRET efficiencies being smaller with 7–10% (on the absolute scale).

Please cite this article as: T. Ungvári, et al., Perrin and Förster unified: Dual-laser triple-polarization FRET (3polFRET) for interactions at the Förster-distance and beyond, Biochim. Biophys. Acta (2016), http://dx.doi.org/10.1016/j.bbamcr.2016.02.002

Table 1
FRET-resolved associated fractions of donors (f) in acceptor-titrated intramolecular FRET between MHCI subunits on JY cells.

FRET-pairs				FRET-fraction (%)	FRET efficiency (%)	Donor anisotropies[d]			Calculated according to Perrin-model with r_0 at $f_0 = 100\%$[e]	
Donor: xFITC-conjugated[a]		Acceptor: Alexa-Fluor 546-conjugated[a]								
mAb_1	$Antigen_1$	mAb_2	$Antigen_2$	f_0[b]	E[c]	r	r_1	r_0	$r_{1,calc}$	f
Part A										
L368	β_2m	W6/32(1)	MHCI h.c.	12.5 ± 1.3	5.2 ± 0.4[f]	0.138 ± 0.012	0.139 ± 0.008	−0.005 ± 0.006	0.139 ± 0.013	1.3 ± 0.9
		W6/32(2)		37.4 ± 3.0	14.7 ± 1.2		0.143 ± 0.010	0.135 ± 0.016	0.143 ± 0.012	7.9 ± 1.5
		W6/32(3)		75.0 ± 5.5	23.3 ± 2.0		0.147 ± 0.011	0.164 ± 0.012	0.145 ± 0.015	79.0 ± 6.0
		W6/32(4)		100.0 ± 8.5	29.6 ± 3.0		0.151 ± 0.012	0.172 ± 0.011	0.148 ± 0.013	92.6 ± 8.3
Part B										
W6/32	MHCI h.c.	L368(1)	β_2m	6.5 ± 0.5	4.2 ± 0.4	0.123 ± 0.010	0.126 ± 0.010	−0.048 ± 0.058	0.149 ± 0.015	0.6 ± 0.7
		L368(2)		23.6 ± 1.4	7.6 ± 0.6		0.127 ± 0.008	0.059 ± 0.030	0.126 ± 0.011	4.2 ± 1.4
		L368(3)		46.6 ± 3.7	13.1 ± 1.1		0.128 ± 0.009	0.150 ± 0.012	0.128 ± 0.012	18.2 ± 1.5
		L368(4)		100.0 ± 9.0	22.2 ± 1.6		0.135 ± 0.012	0.190 ± 0.013	0.133 ± 0.014	84.6 ± 8.5

a) Labeling ratios (L) for the antibodies are listed in parentheses: donor conjugated L368 (3.9), W6/32 (3.71); acceptor conjugated L368 (2.1), W6/32 (2.8)
b) FRET-fractions f_0, for the light chain-heavy chain subunits of the MHCI with 1:1 stoichiometry, have been adjusted by the added amount of acceptor mAbs. They have been computed as $f_0 = (\varepsilon_d \cdot L_d \cdot S_2 \cdot I_a)/(\alpha \cdot \varepsilon_a \cdot L_a \cdot I_d)$, where the ε-values are the molar decadic absorption coefficients for the donor and acceptor at the wavelength of the donor excitation, L-values are the labeling ratios of mAbs, I_a and I_d are intensities for the directly excited acceptor and unquenched donor on the FRET sample, and α is spectroscopic and optical constant for calibration of FRET (d: donor, a: acceptor)
c) E means FRET efficiency determined from the total donor and acceptor intensities according to the standard FCET formalism (Eqs. 1s–5s, in *Supporting information*)
d) r, fluorescence anisotropy of the sample labeled with only the donor. r_1, fluorescence anisotropy of the sample labeled with both donor and acceptor, which depend on both FRET efficiency (E) and clustered donor fraction (f_0). Starting limiting anisotropies r_0 have been determined with the Perrin-model (Eqs. (15)–(17)) with f_0, E, r, r_1 as input parameters
e) These parameters have been determined according to the Perrin-model (Eqs. (15)–(17)) by using r_0 value of the donor determined when $f_0 = 100\%$
f) Data indicate means with their standard errors (SEM) determined on 3 different measurements

Besides the standard application for describing conformational states, the r_0 and σ rotational constants deduced in the knowledge of f, can be further used e.g. for computation of the orientation factor. Alternatively, the σ rotational constant can be an indicator of an extra depolarization of two nearby donors due to homo-FRET in addition to rotational motion, as exemplified by the Perrin-analysis of a triple-FRET system – comprised of 2 donors and 1 acceptor bound the MHCII molecule and to the 2 subunits of MHCI – considered in sections "Orientation factor" and "Hetero-FRET induced homo-FRET relief in receptor trimers" and in Tables 1s, 2s, 3s, in the *Supporting information*.

3.2.2. Polarized FRET-indices

The hybrid parameters computed from the FRET efficiency and the r and $r'(=r_1)$ anisotropies (in Table 1) are listed in Table 2 for the MHCI light chain-heavy chain FRET systems considered above. We constructed these quantities, in the hope of finding a sensitive indicator of conformational changes. Consulting Table 2, Part A, a finite (nonzero) value of anisotropy splits the series of E values into 4 series around the E values, with the largest shifts (zero-offsets) in E_1 and E_4, and with the smallest ones in E_2 and E_3. As also can be revealed, while the size of shifts for E_1 and E_2 are determined by the magnitude of anisotropies r and r′, for E_2 and E_3 the ratio of r′ and r, leading to shifts much smaller in E_2 and E_3 than in E_1 and E_4. Experimental distributions of E_1 and E_4 are shown in Fig. 4 Panel E. The sensitivity factors obtainable by differentiating the FRET-indices with respect to E, determining both the shifts and range of the different indices are the following (see also *Supporting information*), for Part A: E_1, $(1 + 2r')/(1 - r) = 1.48–1.51$; E_2, $(1 + 2r')/(1 + 2r) = 1.002–1.02$; E_3, $(1 - r')/(1 - r) = 0.985–0.999$; E_4, $(1 - r')/(1 + 2r) = 0.665–0.675$; for Part B: E_1, $(1 + 2r')/(1 - r) = 1.43–1.45$; E_2, $(1 + 2r')/(1 + 2r) = 1.005–1.02$; E_3, $(1 - r')/(1 - r) = 0.986–0.997$; E_4, $(1 - r')/(1 + 2r) = 0.69–0.7$. These data imply a 40–50% increase in range and shift for E_1 (as compared to E) a 30–35% reduction in range and shift for E_4, and small shifts and changes in range for E_2 and E_3. The largest deviations from E for E_2 and E_3 are seen at

Table 2
Polarized FRET-indices (E_1–E_4) measured for acceptor-titrated intramolecular FRET between the MHCI subunits on JY cells.

FRET-pairs				Polarized FRET-indices (%)[b]			
Donor: xFITC-conjugated[a]		Acceptor: Alexa-Fluor 546-conjugated[a]					
mAb_1	$Antigen_1$	mAb_2	$Antigen_2$	E_1	E_2	E_3	E_4
Part A							
L368	β_2m	W6/32(1)	MHCI h.c.	−40.3 ± 3.2 [c]	5.1 ± 0.5	5.3 ± 0.5	36.0 ± 3.0
		W6/32(2)		−27.0 ± 2.6	14.2 ± 1.1	15.0 ± 1.2	42.6 ± 3.8
		W6/32(3)		−15.3 ± 1.6	22.1 ± 1.9	24.0 ± 2.2	48.6 ± 4.3
		W6/32(4)		−6.0 ± 0.5	28.4 ± 2.5	30.5 ± 3.0	53.2 ± 4.6
Part B							
W6/32	MHCI h.c.	L368(1)	β_2m	−36.7 ± 3.0	3.8 ± 0.4	4.5 ± 0.4	32.8 ± 3.2
		L368(2)		−31.9 ± 3.2	7.2 ± 0.6	7.9 ± 0.8	35.2 ± 3.7
		L368(3)		−24.3 ± 2.4	12.5 ± 0.9	13.6 ± 1.1	39.3 ± 3.6
		L368(4)		−12.3 ± 1.0	20.9 ± 1.7	23.0 ± 2.0	45.8 ± 3.8

a) Labeling ratios (L) for the antibodies are listed in parentheses: donor conjugated L368 (3.9), W6/32 (3.71); acceptor conjugated L368 (2.1), W6/32 (2.8).
b) Polarized FRET-indices (E_1-E_4) were determined by using E, r and r_1 according to Eqs. (37)–(40). Total association of donors ($f_0 = 1$) was also assumed, when $r_1 = r'$. While the deviation of E_2 and E_3 indicates the degree of enhancement of donor anisotropy due to FRET, i.e. the presence of rotational modes on the timescale of FRET, the deviation of E_1 and E_4 indicates the presence of anisotropy itself, i.e. the lack of rotational modes on the time scale of fluorescence. The absolute range of FRET efficiency is dilated by E_1, and compressed by E_4 with with ~30%.
c) Data indicate means with their standard errors (SEM) determined on 3 different measurements. A similar set of data has been compiled for a two donors-one acceptor system in Table 2s in *Supporting information*.

Please cite this article as: T. Ungvári, et al., Perrin and Förster unified: Dual-laser triple-polarization FRET (3polFRET) for interactions at the Förster-distance and beyond, Biochim. Biophys. Acta (2016), http://dx.doi.org/10.1016/j.bbamcr.2016.02.002

saturating amount of acceptor, when the differences between r and r′ = r_1 are the largest. Based on these calculations, in the data sets of Table 2, E_1 seems to have the aimed enhanced conformational sensitivity. FRET-indices could be applied also for homo-FRET. Pertinent data are shown in Table 3s, in *Supporting information*.

3.2.3. Acceptor anisotropies and orientation factor for FRET (κ^2)

The necessary ingredients for the determination of the limits of orientation factor in the framework of the "Dale-Eisinger analysis" are the (zero-time) limiting anisotropies for the donor, acceptor, and for the sensitized emission, from which the corresponding "axial depolarization factors" are computed (see *Supporting information* for details) [6–9,34,35]. However, from these 3 unknowns only the donor limiting anisotropy and σ parameter can be determined from the donor Perrin-plots in the framework of 3polFRET, the remaining 2 are computed by assuming that (i) the acceptor has the same rotational correlation time as the donor ($\phi_a = \phi_d$), and (ii) the σ rotational constant for the acceptor (σ_a) is reduced in proportion to the smaller lifetime of the acceptor: $\sigma_a = \tau_a\sigma_d/\tau_d$. With this restriction, in the knowledge of the anisotropies of sensitized and directly excited emissions of acceptor (r_{et}, r_a), the axial depolarization factors of acceptor can be estimated. This consideration underscores the importance of $r_{et.}$ and r_a, besides the donor anisotropies r and r_1. These parameters are listed in Table 3 together with the deduced orientation factor limits for the previously considered FRET titrations of MHCI. Pertinent distributions are shown in Fig. 4 Panel D. By inspecting Part A, the lower limit for κ^2 decreases, and the upper one is increasing with the increasing associated fraction. These changes can be attributed to two effects: (i) For the lowest two associated fractions, the r_0 values are under-estimated (Table 1, Part A) and (ii) at the same time the r_a values decrease for the whole range of associated fraction, supposedly due to increasing homo-FRET. Essentially the same behavior of the orientation factor limits can be read off from Part B of Table 2.

As to the values of $r_{et.}$, these are consistently close to zero, with rare exceptions only at the smallest FRET efficiencies, where the larger negative deviations can be attributed to the small value of sensitized emission, and consequently to the small value of the product (I_1A') occurring in the denominator for the formula of $r_{et.}$ in Eq. (13), see also Eq. 14s in *Supporting information*. The dropping of r_a with the increasing acceptor concentration can be traced to the increasing role of homo-FRET in depolarizing acceptor emission. By comparing these r_a values in the presence of donor with those observed in the absence of donor (r_3 for single acceptor-labeled samples, not shown), no significant difference can be noticed, implying that the reason for the anisotropy increase is not a donor-induced increase in rigidity of the dye-holding protein matrix ("solidification").

4. Discussion

4.1. The 3polFRET scheme combines proximity and mobility

The conventional dual laser FCET methodology [10–16] has been extended with polarization optics to make possible a more complete, "close-to global" approach of FRET determination. This novel platform pushes the range of capabilities of FCET towards direct methods of fluorescence lifetime measurements – the different FLIM techniques – by enabling the determination of FRET-fraction, rotational properties of the donor and acceptor as well as the determination of the limits of orientation factor for FRET (κ^2) [26,29,31]. This methodology opens the way towards a complete description of FRET systems – by simultaneously measuring FRET efficiency and orientation factor – on relatively easily and cheaply realizable systems like flow cytometry and imaging microscopes operating in the steady state. Realization of the method in flow cytometry has a special impetus, due to its high-throughput nature i.e. the capability for filtering out rare cell events from a huge background population in a short time.

Generally these parameters can be determined in the time- or frequency-domain by using some fluorescence lifetime measuring scheme. However, in the 3polFRET approach they are determined in the steady state from the primarily measured FRET efficiency (E), donor anisotropy in the presence of FRET (r_1), anisotropy of sensitized and directly excited emissions of acceptor (r_{et}, r_a). The determination of FRET-fraction and rotational constants is based on the FRET dependence of the donor anisotropy (r_1) via the Perrin-equation, both FRET efficiency and donor anisotropy involving the same donor lifetime. The ingredients of the orientation factor, the axial depolarization factor for the donor, acceptor and FRET are then determined from the rotational constants of the donor, and the $r_{et.}$ and r_a anisotropies. This methodology is rapid because – notwithstanding now the different S-factors and α (see them in *Supporting information*) – the necessary anisotropies (r_1, r_{et}, r_a) are determined on a single double-labeled FRET sample, together with the FRET efficiency (E). Furthermore, it is cost-effective and relatively simply realizable in flow cytometers and fluorescence microscopes, requiring only wave retarders and polarization beam- (or image-) splitters in the excitation and detection ports [17].

Table 3
FRET-resolved limits of orientation factor (κ^2) measured for acceptor-titrated intramolecular FRET between the MHCI subunits on JY cells.

FRET-pairs				Acceptor anisotropies[b]		Lower and upper limits of orientation factor[c]	
Donor: xFITC-conjugated[a]		Acceptor: Alexa-Fluor 546-conjugated[a]					
mAb_1	$Antigen_1$	mAb_2	$Antigen_2$	r_{et}	r_a	κ^2_{min}	κ^2_{max}
Part A							
L368	β_2m	W6/32(1)	MHCI h.c.	−0.107 ± 0.100 [d]	0.186 ± 0.015	0.60 ± 0.05	1.40 ± 0.12
		W6/32(2)		0.014 ± 0.010	0.181 ± 0.016	0.43 ± 0.03	2.20 ± 0.20
		W6/32(3)		0.006 ± 0.008	0.177 ± 0.014	0.35 ± 0.05	2.45 ± 0.20
		W6/32(4)		0.011 ± 0.010	0.174 ± 0.017	0.32 ± 0.04	2.49 ± 0.20
Part B							
W6/32	MHCI h.c.	L368(1)	β_2m	−0.033 ± 0.100	0.191 ± 0.015	0.61 ± 0.06	1.27 ± 0.13
		L368(2)		0.006 ± 0.010	0.180 ± 0.014	0.46 ± 0.04	1.95 ± 0.20
		L368(3)		0.004 ± 0.010	0.174 ± 0.012	0.37 ± 0.04	2.44 ± 0.20
		L368(4)		−0.005 ± 0.020	0.173 ± 0.016	0.28 ± 0.02	2.61 ± 0.25

a) Labeling ratios (L) for the antibodies are listed in parentheses: donor conjugated L368 (3.9), W6/32 (3.71); acceptor conjugated L368 (2.1), W6/32 (2.8).
b) Acceptor anisotropies $r_{et.}$ and r_a were calculated according to Eqs. (13), (14).
c) Lower and upper limits for the orientation factor κ^2_{min} and κ^2_{max} were computed according to Eqs. 29s and 30s in *Supporting information*.
d) Data indicate means with their standard errors (SEM) determined on 3 different measurements. A similar set of data has been compiled for a two donors-one acceptor system in Table 4s in *Supporting information*.

Please cite this article as: T. Ungvári, et al., Perrin and Förster unified: Dual-laser triple-polarization FRET (3polFRET) for interactions at the Förster-distance and beyond, Biochim. Biophys. Acta (2016), http://dx.doi.org/10.1016/j.bbamcr.2016.02.002

4.2. Polarization FRET-indices unify FRET and polarization for sensing conformational change

Apart from the determination of FRET-fraction and orientation factor, this global approach for FRET may also be promising for a more complete description of conformational changes, due to the fact that 3 conformation sensitive parameters – the r_1, $r_{et.}$, and r_a anisotropies – are detected in addition to the FRET efficiency E. In this respect our 3polFRET approach can also be envisioned as the nano-optical realization of the principle formulated in the Chasles' theorem of mechanics (Fig. 5) [45] stating that the general motion of a body – like those in a conformational change – can always be decomposed to the sum of a translation and a rotation, with the translation corresponding to FRET and rotations to the anisotropies. However – besides this direct scheme, in which anisotropies and FRET are separately treated – an indirect scheme can also exist, when the effects of FRET and rotations appear in a combined manner. In the indirect scheme, FRET efficiency is computed not from the total intensities, but from the polarized intensity components of e.g. the donor intensity, giving rise to 4 different "FRET-indeces" E_1-E_4 (Eqs. (37)–(40)), taking into account all possible pairings of the excitation and detection polarization directions. The evolution of these indices can also be envisioned as splitting up the FRET efficiency E into four – not independent (Eq. 28 s in *Supporting information*) – polarized components due to the lack of complete orientational isotropy manifested in the finite (non-zero) donor anisotropy, like in the cases of E_1 and E_4, or due to an increase of donor anisotropy upon FRET, like in the cases of E_2 and E_3. A geometrical representation of the relative positions of the indices in a "generalized anisotropy space" is shown in Fig. 6. After calculating the anisotropy-dependent sensitivity factors in formulae of the 4 indices, E_1 turned to be amenable for application as a conformational index, by enhancing the FRET range with a factor of ~$(1 + 2r')/(1 - r)$, in contrast to the others which compress (E_4, with a factor of ~$(1 - r')/(1 + 2r)$) or influence only a little (E_2, E_3 with factors proportional to ~$r' - r$, the difference of anisotropies) the FRET range (see also in *Supporting information*).

Although the polarized FRET indices E_1-E_4 have been defined for hetero-FRET, they can also be applied in the case of homo-FRET, by taking E as zero, and representing by r the intensity weighted average of anisotropies of samples labeled separately by the different donor-species (no homo-FRET), and by r′, the anisotropy of the sample labeled in a single act with the mixture of the different donors (finite homo-FRET) (see Table 3s in *Supporting information*).

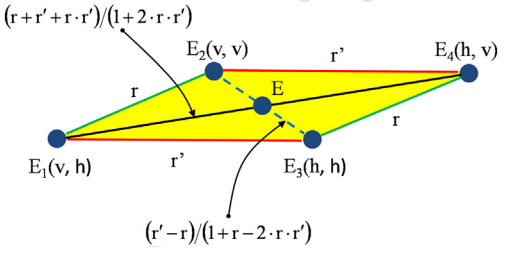

Fig. 6. *Cartoon visualizing the splitting of FRET efficiency E into the polarized FRET index components E_1–E_4.* The FRET indices and E are shown in the space of "generalized anisotropy" (defined by Eq. 23 s in *Supporting information*) with their distances characteristic on the amount of splitting. The smallest deviations are seen between E_2, E_3 and E, being proportional to the FRET-induced donor anisotropy enhancement, r′–r, which is small. For no enhancement (r′ = r) E splits only to E_1 and E_4. For nonzero anisotropies E_1 and E_4 always deviate from E and from each other, with the largest deviation proportional to the sum of the donor anisotropies measured in the absence and presence of FRET, r + r′. For zero anisotropy – quick rotations on the fluorescence time scale – there is no splitting at all. For non-zero r and when r′ > r, the splittings of E into E_1 and E_4 change inversely with FRET efficiency (E) and rotational constant ($\sigma = \tau/\phi$). Although the splittings of E into E_2 and E_3 also change inversely with the FRET efficiency, they change parallel with the rotational constant (σ), see also Fig. 1s, in *Supporting information.*

4.3. Associated fraction for hindered rotations

Rotational motion of dyes tethered to receptors in the cell membrane may be constrained (or hindered) and the limiting anisotropy and rotational correlation time introduced in Eq. (16) are only "apparent" or "effective" values describing rotational motion only crudely. By intuition, keeping the original formulation of the Perrin-model (Eq. (16)) possible hindrance in dye rotation may lead to an under estimation of the rotational constant (σ), and as a consequence an under estimation in the associated donor fraction (f). In contrast to this behavior of associated fraction, the uncertainty in κ^2 (Eqs. 29 s, 30s in *Supporting information*) should not be influenced much, because hindrance mostly affects the rotational correlation time, not the r_0, the quantity governing κ^2.

In the next we attempt to prove this guess analytically by presenting a summary of constrained rotations of tethered dyes (see also in *Supporting information* to [21]). A refined description of donor rotation can be given by an extended form of the Perrin-equation, when in the framework of the "wobbling in a cone" model of rotational depolarization a term describing the "half angle of the rotational cone", the r_∞ limiting anisotropy is also incorporated [26,41,42,46]:

$$r - r_\infty = (r_{0,h} - r_\infty)/(1 + \sigma_h). \quad (41)$$

Here $r_{0,h}$ and σ_h, the limiting anisotropy and rotational constants in the presence of hindrance, are defined analogously to the unhindered case (Eq. (18)). The degree of hindrance is expressed by r_∞, and it can be given as a percentage (ξ) of the limiting anisotropy $r_{0,h}$:

$$\xi \equiv r_\infty / r_{0,h} \ . \quad (42)$$

With ξ, Eq. (41) can be cast in another form more amenable for further analysis:

$$r = r_{0,h} \cdot (1 + \xi \cdot \sigma_h)/(1 + \sigma_h). \quad (43)$$

This equation is valid for the donor in the absence of acceptor. It can be seen that at the limit of the unhindered rotator ($\xi = 0$), it goes into the original Perrin-equation (Eq. (16)). In the presence of acceptor after taking into account the lifetime-reduction due to FRET, Eq. (43) assumes a form analogous to Eq. (17):

$$r' = r_{0,h} \cdot [1 + \xi \cdot \sigma_h \cdot (1 - E)]/[1 + \sigma_h \cdot (1 - E)]. \quad (44)$$

As to the associated fraction (f) the pertinent formulae, Eq. (19) defining f the, and Eq. (15) the average anisotropy of the donor in the presence of acceptor, can be taken as valid also here. The procedure of associated fraction determination remains also the same, with the exception that now Eqs. (43), (44) should be plugged into Eq. (15) for the donor anisotropy average, instead of Eqs. (16), (17). The procedure can be applied also here in two ways: Either the rotational constants are determined in the knowledge of the associated fraction (f) ("forward direction"), or vice versa, the associated fraction (f) is determined in the knowledge of the rotational constants ($r_{0,h}$, σ_h, ξ) ("backward direction"). In both cases the input, measured parameters are the donor-only anisotropy (r), the donor anisotropy in the presence of acceptor (r_1), and the FRET efficiency (E). The associated fraction (f) may be known in advance from presumptions on the structure. The rotational constants may be obtained even is the steady state by non-linear fitting of Eq. (44) to the empirical anisotropy vs. fluorescence lifetime curves. Lifetime changes can be achieved by FRET with a series of acceptor antibodies of increasing labeling ratio, or increasing labeling concentration, or by some other quenching process, e.g. quenching with KI [41,44].

If the rotational constants are the known quantities ("backward direction"), e.g. $r_{0,h}$ and ξ, then calculation of E_0, and f goes also via

introducing the "helper quantity" analogous to σ_{app} (Eq. (20)), but designated now as $\sigma_{app,h}$:

$$\sigma_{app,h} \equiv (r_1 - r)/[r - E \cdot \xi \cdot r_{0,h} - r_1 \cdot (1-E)]. \quad (45)$$

By inspecting Eq. (45) it can be seen that in the limiting case of zero for ξ implying no hindrance, $\sigma_{app,h}$ goes into σ_{app} of Eq. (20) as it should do. With $\sigma_{app,h}$ and σ_h, the solution for E_0 of Eq. (15) is similar in structure to Eq. (21):

$$E_{0,h} = 1 - (1-E) \cdot \sigma_{app,h}/\sigma_h. \quad (46)$$

The solution for f is obtained from Eq. (19) after plugging $E_{0,h}$ of Eq. (46) in place of E_0:

$$f_h = E/[1 - (1-E) \cdot \sigma_{app,h}/\sigma_h]. \quad (47)$$

In the reversed ("forward") direction, the solution for the rotational constants σ_h, $r_{0,h}$ can be obtained by first expressing σ_h from Eq. (46) as,

$$\sigma_h = f \cdot (1-E) \cdot \sigma_{app,h}/(f-E), \quad (48)$$

then putting σ_h into Eq. (43), from which $r_{0,h}$ can be expressed as:

$$r_{0,h} = r \cdot [1 + f \cdot (1-E) \cdot \sigma_{app}/(f-E)]/[1 + \xi \cdot f \cdot (1-E) \cdot \sigma_{app}/(f-E) \ .] \quad (49)$$

To see the effect of hindrance on the f and E_0 clearly, the following relationship between the $(\sigma_{app,h}/\sigma_h)$ and (σ_{app}/σ) ratios can be deduced by taking into account the definitions for σ_h and $\sigma_{app,h}$ (Eqs. (43), (45)) and for σ and σ_{app} (Eqs. (16), (20)):

$$\sigma_{app,h}/\sigma_h = (\sigma_{app}/\sigma) \cdot \{1 + (r_1/r - 1) \cdot r_\infty \cdot (1-E)/[r - E \cdot r_\infty - r_1 \cdot (1-E)]\}, \quad (50)$$

where $r_0 = r_{0,h}$ has also been assumed.

Decisive is that the 2nd term in the braces is positive, because the r-containing term in it is larger than the term containing r_1. The positivity of the 2nd term implies the following inequality:

$$\sigma_{app,h}/\sigma_h > \sigma_{app}/\sigma. \quad (51)$$

Based on the inequality in Eq. (51), hindrance against rotation decreases E_0 (from Eqs. (21), (46) for E_0, $E_{0,h}$), and increases f (from Eqs. (22), (46) for f, f_h):

$$E_{0,h} < E_0, f_h > f. \quad (52)$$

That the associated fraction f should increase with hindrance can be reasoned qualitatively as follows: in Eqs. (43) and (44) hindrance appears as a negative feedback effect opposing the increase of anisotropy due to lifetime reduction. Because due to the presence of the 1 − E factor in r′ (Eq. (44)) the opposing effect of ξ is relatively suppressed in r′ as compared to r (Eq. (43)), implying that by increasing ξ the weight in the average donor anisotropy r_1 (Eq. (15)) is shifted towards the term containing r. However, r_1 is a measured constant, which implies that the multiplying factor of r (1-f) should reduce and the factor of r′ (f) increase in Eq. (15). This means that f should be increased with increasing ξ. Accordingly, E_0 should decrease based on Eq. (19).

The connection between the linear approximation, i.e. the original Perrin formulation forced to describe hindered rotator data and the hindered model of Eq. (43) can be revealed by transforming Eq. (43) to the form of Eq. (16):

$$r' = r_{0,h}/[1 + \sigma_h \cdot (1-\xi)/(1 + \xi \cdot \sigma_h)] \ . \quad (53)$$

Comparing Eqs. (53) and (16), it can be seen that: (i) Eq. (53) describes an unhindered rotator possessing a lifetime-dependent effective rotational correlation time, and effective rotational constant:

$$\sigma_{eff} \equiv \sigma_h \cdot (1-\xi)/(1 + \xi \cdot \sigma_h) \ . \quad (54)$$

The lifetime dependence of $\sigma_{h,eff}$ is dictated by ξ, as a "coupling constant", in the denominator. (ii) Because the multiplication factor of σ_h is smaller than unity, hindrance reduces the effective speed of rotation, as expected. (iii) Because the numerator of r′ in Eq. (53) is independent of ξ, the forced linear fitting (with Eq. (16)) of the hindered rotator supplies approximately the true $r_{0,h}$ limiting anisotropy, i.e. $r_0 \approx r_{0,h}$. The approximation is the better, the smaller ξ is.

According to the rotational data obtained by rFLIM technique on the same mAbs and cells (Fig. 2*s* in *Supporting information* to [21]), the ξ parameter expressing hindrance varies around 23%. By using this value for ξ in computing associated fractions according to Eq. (47) with the data of Table 1, ~20%-larger f values result for $r_0 = 0.2$, and ~10%-larger for $r_0 = 0.25$. This calculation indicates also that, the effect of hindrance depends also on the value of the limiting anisotropy. According to both flow cytometric and rFLIM observations, the σ_{eff} values (at 488 or 514 nm) are around 0.4 [19,21]. By using 23% for ξ in Eq. (54), a value of 0.53 can be obtained for σ_h, implying that the $(\xi\sigma_h)$ term can be neglected compared to 1 (being 0.11), and $\sigma_{eff} \approx \sigma_h(1-\xi)$. This also shows that the $r_0 \approx r_{0,h}$ is also a reasonable approximation.

4.4. Calibration of FRET by determining α

In the calculations we followed the conventional way of FCET calculation when the α factor [48,49] balancing the different sensitivities of the donor and acceptor channels has been determined from suitable single-labeled samples: From samples labeled with only donor and acceptor in a known acceptor-to-donor concentration ratio, ensured e.g. by a 1:1 donor-acceptor stoichiometry, as in the present case of the two subunits of the MHCI receptor. Afterwards, E and I_d are computed with α. (In contrast to E and I_d, the intensity I_a, proportional with the acceptor concentration, is independent from α.) However, a "reversed scheme" can also be imagined, when the α factor is the aimed parameter. When the limiting anisotropy and the associated fraction of the donor are known in advance, FRET efficiency E can be computed on the donor side with the Perrin-model. Then the α factor is fixed by the condition that the FRET efficiency of the FCET formalism should be the same as the one obtained by the Perrin-model. Reversely, by knowing α, validity of the Perrin-model could be checked by comparing two FRET efficiencies: one computed with the FCET method as standard, and the other one computed with the Perrin-model. The precondition of this approach is that donor anisotropy should be sensitive on FRET, i.e. rotational modes on the time scale of FRET – "transfer rotational modes" – should be present [19].

4.5. Incomplete polFRET schemes: 1polFRET, 2polFRET approaches

If the acceptor anisotropies are not important, a simplified polFRET scheme can be applied, when the polarized intensity components are detected only for the donor, and the total intensities I_2, I_3 for the acceptor (1polFRET). This scheme can be applied e.g. when the associated donor fraction or the rotational constants of the donor are important, and for the determination of α in the aforementioned way. In another simplification, only a single laser is used at the donor's excitation wavelength ("single-laser polFRET" or "dual-polarization FRET (2polFRET)", discussed in [21]). In this version of FRET determination, the I_3 intensity necessary for the solution of the FCET problem in addition to I_1 and I_2 – i.e. for finding E, I_d, I_a – is replaced by the acceptor anisotropy r_a' in the presence of donor. The reliability of the method is determined by the condition that the anisotropy of sensitized emission (r_{et}) should be a known value, e.g. zero. Although the method rests on the acceptor

Please cite this article as: T. Ungvári, et al., Perrin and Förster unified: Dual-laser triple-polarization FRET (3polFRET) for interactions at the Förster-distance and beyond, Biochim. Biophys. Acta (2016), http://dx.doi.org/10.1016/j.bbamcr.2016.02.002

anisotropy r_a' measured in the presence of FRET, the detection of the donor anisotropy r_1 is also necessary. It is needed for correcting donor's cross-talk in the acceptor anisotropy, see Eqs. 12s and 13s in *Supporting information*. The main differences between the earlier "single laser polFRET" and the present approach, 3polFRET are that in the latter: (i) No assumption on the anisotropy of sensitized emission is made. (ii) Directly excited acceptor anisotropy (r_a) is measured, making possible checking for the sterical effect of the presence of the donor-bearing ligand ("sterical hindrance"). (iii) Because of the simultaneous determination of the donor anisotropy (r_1), and the 2 acceptor anisotropies – sensitized emission (r_{et}) and directly excited (r_a) – with FRET efficiency (E), the latter approach makes feasible a more complete description of the FRET system, enabling also the orientation factor (κ^2). In the knowledge of the orientation factor for FRET, computation of distance distributions may be attempted (see in *Supporting information*). (iv) New indicators of receptor dynamics, called polarization FRET-indices (E_1–E_4) may be introduced, some of which with the promise for an enhanced sensitivity in detecting conformational changes.

4.6. Triple-anisotropy correlations for FRET and non-FRET interactions: κ^2 in a wider context

The 3polFRET method has been introduced as a "natural extension" of the conventional FCET method from the unpolarized optical regime to the polarized one. However, it might have a broader field of application, because the simultaneous measurement of 3 anisotropies does not necessitate the presence of FRET. It can be used for monitoring 2–3 different spectral channels of a single fluorophore or up to 3 different fluorophores with "well separable spectral ranges", e.g. quantum dots (QDs) [21,30]. Consequently it belongs to the "spectral anisotropy" category recently introduced by Esposito et al. [29].

Another related technique recently introduced in the field of biosensing is "dual-polarization interferometry" (DPI) [50]. The name of this technique suggests as if two different pairs of polarization channels – the two polarized components of say channel#1 and channel#2 – would be applied simultaneously. However, in the present form of the technique the interference between two polarized components of a single channel is exploited, one polarized component serving as the probe beam, and the other one as the reference beam for the interference. This technique can also be extended with involvement new polarization channels for new parameters.

As to the relevant non-FRET interactions, e.g. correlated membrane events elicited by spreading membrane potential in an axon ("solitary waves"), or osmotic pressure in a cell, can be mentioned [51]. Collective motions of DNA can also be monitored by selectively labeling with 3 different dyes. According to the Perrin-equation (Eq. (15)) basically the correlations between 3 different lifetimes and rotational correlation times can be detected in these cases. In this respect the method shows some similarity to the astronomic observations where correlations between intensities or intensity anisotropies of light waves arriving from distal points are measured [52].

Accordingly, the interpretation of κ^2 can also be put in a wider context, conceiving it as a purely geometrical measure of the relative orientational distributions of two dipole ensembles. This can be made e.g. by taking Eqs. 29s and 30s (in *Supporting information*) for κ^2_{min} and κ^2_{max} as the definitions, which make sense independently whether FRET is measured or not.

4.7. Earlier works on FRET determination from dual- and triple-anisotropy correlations

The concept of simultaneously measuring FRET with the donor and acceptor anisotropies has already been applied in the field of single-molecule fluorescence [27,53] where the occurrence of a single FRET event is justified by the detection of the anti-correlations of donor and acceptor intensities and anisotropies for a given donor-acceptor pair. Here the need for the dual-anisotropy approach for FRET detection naturally arises because fluctuations of the orientation factor for FRET (κ^2) do not average out at this statistical level. In a very elegant work in the field of wide-field steady-state fluorescence imaging, Mattheyses et al. [28] have already used the triple-polarization concept for a robust determination of FRET efficiency and the donor and acceptor concentrations from only a single camera exposure for all the 3 detected signals with the aim of rapid identification of binding events in biosensing detection schemes. Although the terms of their matrix formalism should correspond to our terms (Eqs. (11), (12)), their meaning and implications regarding the dynamics of the FRET system have been left burried.

4.8. The polarization bias of FRET efficiency

Our formalism is amenable to estimate the committed errors in the FRET efficiency determined either only via the donor intensity (i.e. the efficiency of donor quenching) or from the sensitized emission of acceptor when the intensities are detected without a polarizer with vertically polarized excitation. This error is due to the fact that when FRET is detected perpendicularly to the direction of excitation with linearly polarized light, the detected intensities are not the total ones, which are independent from polarization, but only partial intensities showing some polarization dependence [42,43]. This polarization error can be circumvented by either exciting via a linear polarizer set at the magic angle (54.7°) relative to polarization direction of the detection, or detecting through a polarizer set at the magic angle relative to the polarization direction of excitation. Detecting perpendicularly to the illumination direction, the polarization dependence also sustains even when excitation is with depolarized light. This effect has been exploited for a high-sensitive detection of polarization in [54].

4.9. κ^2 as a tool for controlling FRET

The most fundamental property of κ^2 is that in the absence of its knowledge the FRET efficiency cannot be translated into distance, the aimed parameter in most of the applications of FRET. We followed the route of κ^2 determination via the depolarization factors (please see it in *Supporting information*) as originally published by Dale et al. [6]. They also were the first in calling the attention for treating FRET and polarization in a unified fashion. Depolarization factors, the input parameters of κ^2 can also be determined by excitation angle-resolved intensity measurements in a confocal microscope [34]. A possibility for narrowing the uncertainty of κ^2 has recently published in [35].

Besides the above "passive role" of κ^2 played in proximity determinations, it can also be exploited "actively", for controlling FRET directionality. This may be based on that κ^2 expresses the directionality of interaction by the donor and acceptor, being a factor characteristic for the orientational distribution of the donor's local field [7–9]. Orientation of FRET process is a problem of engineering the distribution of the donor's local field. This can be accomplished e.g. by the type of donor transition, or by putting a plasmonic nano-particle or some other boundary surface in the vicinity of donor, modifying the distribution of the donor's local field [55].

A special type of donor transition amenable for the above purpose is the rotating donor dipole [56]. Emitters of natural chirality belong to this class of emitters. However some long lasting chirality for officially not chiral emitters can also be expected after excitation with circularly polarized light based conservation of angular momentum (helicity) [57]. Conservation of angular momentum is manifested in a recently discovered series of phenomena with circularly polarized light classified as spin orbit interaction (SOI) of light [58]. SOI expresses a deep connection between polarization and geometry called geometric (or Pancharatnam–Berry) phase. The deep consequence of geometric phase is that the behavior of electrodynamics may be governed by spatial geometry and factors affecting the geometry. Because FRET in inherently connected to geometry and polarization, manifestations of angular momentum conservation

Please cite this article as: T. Ungvári, et al., Perrin and Förster unified: Dual-laser triple-polarization FRET (3polFRET) for interactions at the Förster-distance and beyond, Biochim. Biophys. Acta (2016), http://dx.doi.org/10.1016/j.bbamcr.2016.02.002

can also be expected for FRET [57–59]. Circularly polarized light, as a depolarized way of excitation can also lead to modification of FRET by enabling more donors for the acceptors to quench when acceptor dipole orientations are anisotropically distributed [34,60].

4.10. Extending 3polFRET into the domain of circular polarization

Besides linear polarization, circular polarization can also be used for representing the polarization state of matter [61]. E.g. the linearly polarized state can be conceived as the coherent superposition of two counter-rotating circularly polarized state. In the framework of the "circular-base" description of polarization, optical activity is explained by a phase shift between the left- and right-rotating circular components leading to changing the direction of linear polarization. In this respect the depolarization of sensitized emission during FRET can also be visualized as a kind of "optical activity of FRET". The complete description of polarization state of light requires specifying also its circular content besides the linear one.

These questions and the ones detailed above necessitate pushing 3polFRET into the domain of circular polarization [62]. This may be accomplished by introducing circular polarizers (quarter-wave plates) into the excitation and detection paths besides the linear polarizers, enabling the full description of polarization state of fluorescence with the components of the 4-D Stokes-vector [61].

5. Conclusion

Dual-laser flow cytometric FRET method (FCET) has been extended for a detailed quantitation of stoichiometry and dynamics of receptor clusters by the detection of polarized intensity components of the donor and acceptor. The new approach (3polFRET) enables a complete description of FRET systems in the multiplexing and high-throughput conditions of flow cytometry. The capabilities of the new method have been illustrated with the determination of donor's associated fraction and rotational dynamics, and orientation factor for FRET-systems comprised of the two subunits of the MHCI molecule with changing acceptor level. Hetero-FRET-induced "relief of homo-FRET" has been detected in a 2 donors-1 acceptor system comprised of the two subunits of MHCI as the donors and MHCII as the acceptor by analysis of donor Perrin-plots. For a more sensitive detection of conformational changes hybrid parameters, the polarized-FRET indices have been introduced by mixing FRET efficiency and donor anisotropy. One of them, E_1 has been shown to extend the range of FRET substantially. Although the method has been worked out for a flow cytometer, it can be realized also in fluorescence microscopes capable for triple-channel polarization imaging. Dynamical information can be gathered with this method, similar to that with anisotropy FLIM (rFLIM), but at the steady state, which is simpler and at a lower cost. Realizing it in flow conditions the much higher speed of data acquisition and the increased statistical precision are the other merits.

Q3

Q4

Uncited references

[37,38,47]

Acknowledgements

Financial support for this work was provided by TÁMOP-4.2.2.A-11/1/KONV-2012-0045 project co-financed by the European Union and the European Social Fund, and OTKA Bridging Fund support OSTRAT/810/213 by the University of Debrecen. One of the authors (L.B.) is wishing to express the appreciation for Imre Péntek (Nagykőrös, Hungary) for a fascinating first introduction into the field of wave polarization.

Appendix A. Supplementary data

Supplementary data to this article can be found online at http://dx.doi.org/10.1016/j.bbamcr.2016.02.002.

References

[1] B.W. van der Meer, in: I. Medinzt, N. Hildebrandt (Eds.), . Ch. 3 Förster theory. in FRET — Förster resonance energy transfer: from theory to applications, 1th ed.Wiley-VCH, 2013.
[2] E.A. Jares-Erijman, T.M. Jovin, FRET imaging, Nat. Biotechnol. 21 (11) (2003) 1387–1395.
[3] J.R. Lakowicz, Energy transfer. Ch. 13, Principles of Fluorescence Spectroscopy, Kluwer Academic/Plenum Publishers, New York 1999, pp. 368–391.
[4] Clegg, R.M. 2009. Förster resonance energy transfer-FRET what is it, why do it, and how it's done. Ch. 1 In: FRET and FLIM techniques. Laboratory techniques in biochemistry and molecular biology. vol. 33. TWJ Gadella ed., S Pillai, PC van der Vliet series eds. Elsevier p 1–48.
[5] Periasamy A., R.N. Day (Eds.), Molecular Imaging: FRET Microscopy and Spectroscopy, 1th ed.Academic Press 2011, pp. 1–307.
[6] R.E. Dale, J. Eisinger, W.E. Blumberg, The orientational freedom of molecular probes. The orientation factor in intramolecular energy transfer, Biophys. J. 26 (1979) 161–194.
[7] E. Haas, E. Katchalski-Katzir, I.Z. Steinberg, Effect of orientation of donor and acceptor on the probability of energy transfer involving electronic transitions of mixed polarization, Biochemistry 17 (23) (1978) 5064–5070.
[8] B.W. van der Meer, Orientational aspects in pair energy transfer, in: D.L. Andrews, A.A. Demidov (Eds.), Resonance energy transfer, J. Wiley & Sons, New York 1999, pp. 151–172.
[9] B.W. van der Meer, Kappa-squared: from nuisance to new sense, Rev. Mol. Biotechnol. 82 (2002) 181–196.
[10] L. Trón, J. Szöllősi, S. Damjanovich, S.H. Helliwell, D.J. Arndt-Jovin, T.M. Jovin, Flow cytometric measurements of fluorescence resonance energy transfer on cell surfaces. Quantitative evaluation of the transfer efficiency on a cell-by-cell basis, Biophys. J. 45 (1984) 939–946.
[11] L. Trón, Experimental methods to measure fluorescence resonance energy transfer, in: S. Damjanovich, J. Szöllősi, L. Trón, M. Edidin (Eds.), Mobility And Proximity In Biological Membranes, CRC Press, Boca Raton, FL 1994, pp. 1–47.
[12] J. Szöllősi, S. Damjanovich, L. Mátyus, Application of fluorescence resonance energy transfer in the clinical laboratory: routine and research, Cytometry 34 (1998) 159–179.
[13] J. Szöllősi, S. Damjanovich, M. Balázs, P. Nagy, L. Trón, M.J. Fulwyler, F.M. Brodsky, Physical association between MHC class I and class II molecules detected on the cell surface by flow cytometric energy transfer, J. Immunol. 143 (1989) 208–213.
[14] J. Szöllősi, V. Hořejší, L. Bene, P. Angelisová, S. Damjanovich, Supramolecular complexes of MHC class I, MHC class II, CD20, and Tetraspan molecules (CD53, CD81, and CD82) at the surface of a B cell line JY, J. Immunol. 157 (1996) 2939–2946.
[15] L. Damjanovich, J. Volkó, A. Forgács, W. Hohenberger, L. Bene, Crohn's disease alters MHC-rafts in $CD4^+$ T-cells, Cytometry A 81A (2012) 149–164.
[16] R. Gáspár Jr., P. Bagossi, L. Bene, J. Matkó, J. Szöllősi, J. Tőzsér, L. Fésüs, T.A. Waldmann, S. Damjanovich, Clustering of class I HLA oligomers with CD8 and TCR: three-dimensional models based on fluorescence resonance energy transfer and crystallographic data, J. Immunol. 166 (2001) 5078–5086.
[17] Z. Lakos, Á. Szarka, L. Koszorús, B. Somogyi, Quenching-resolved emission anisotropy: a steady state fluorescence method to study protein dynamics, J. Photoch. Photobiol. B 27 (1995) 55–60.
[18] J. Matkó, A. Jenei, L. Mátyus, M. Ameloot, S. Damjanovich, Mapping of cell surface protein-patterns by combined fluorescence anisotropy and energy transfer measurements, J. Photochem. Photobiol. B. 19 (1) (1993) 69–73.
[19] L. Bene, M.J. Fulwyler, S. Damjanovich, Detection of receptor clustering by flow cytometric fluorescence anisotropy measurements, Cytometry 40 (2000) 292–306.
[20] M. Cohen-Kashi, S. Moshkov, N. Zurgil, M. Deutsch, Fluorescence resonance energy transfer measurements on cell surfaces via fluorescence polarization, Biophys. J. 83 (2002) 1395–1402.
[21] L. Bene, T. Ungvári, R. Fedor, L. Damjanovich, Single-laser polarization FRET (polFRET) on the cell surface, BBA Mol. Cell. Res. 1843 (2014) 3047–3064.
[22] S.S. Chan, D.J. Arndt-Jovin, T.M. Jovin, Proximity of lectin receptors on the cell surface measured by fluorescence energy transfer in a flow system, J. Histochem. Cytochem. 27 (1) (1978) 56–64.
[23] L.W. Runnels, S.F. Scarlata, Theory and application of fluorescence homotransfer to mellitin oligomerization, Biophys. J. 69 (1995) 1569–1583.
[24] L. Bene, J. Szöllősi, G. Szentesi, L. Damjanovich, R. Gáspár Jr., T.A. Waldmann, S. Damjanovich, Detection of receptor trimers on the cell surface by flow cytometric fluorescence energy homotransfer measurements, BBA Mol. Cell Res. 1744 (2005) 176–198.
[25] M.A. Rizzo, D.W. Piston, High-contrast imaging of fluorescent protein FRET by fluorescence polarization microscopy, Biophys. J. Biophys. Lett. (2005), http://dx.doi.org/10.1529/biophysj.104.055442.
[26] A.H.A. Clayton, Q.S. Hanley, D.J. Arndt-Jovin, V. Subramaniam, T.M. Jovin, Dynamic fluorescence anisotropy imaging microscopy in the frequency domain (rFLIM), Biophys. J. 83 (2002) 1631–1649.
[27] L. Cognet, G.S. Harms, G.A. Blab, P.H.M. Lommerse, T. Schmidt, Simultaneous dual-color and dual-polarization imaging of single molecules, Appl. Phys. Lett. 77 (24) (2000) 4052–4054.

Please cite this article as: T. Ungvári, et al., Perrin and Förster unified: Dual-laser triple-polarization FRET (3polFRET) for interactions at the Förster-distance and beyond, Biochim. Biophys. Acta (2016), http://dx.doi.org/10.1016/j.bbamcr.2016.02.002

[28] A.L. Mattheyses, A.D. Hoppe, D. Axelrod, Polarized fluorescence resonance energy transfer microscopy, Biophys. J. 87 (2004) 2787–2797.
[29] A. Esposito, A.N. Bader, S.C. Schlachter, D.J. van den Heuvel, G.S. Kaminski Schierle, A.R. Venkitaraman, C.F. Kaminski, H.C. Gerritsen, Design and application of a confocal microscope for spectrally resolved anisotropy imaging, Opt. Express 19/3 (2011) 2546–2555.
[30] L. Bene, T. Ungvári, R. Fedor, I. Nagy, L. Damjanovich, Dual-laser homo-FRET on the cell surface, BBA MCR 1853 (5) (2015) 1096–1112.
[31] A. Esposito, H.C. Gerritsen, F.S. Wouters, Fluorescence lifetime heterogeneity resolution in the frequency domain by lifetime moments analysis, Biophys. J. 89 (2005) 4286–4299.
[32] A.H.A. Clayton, The polarized AB plot for the frequency-domain analysis and representation of fluorophore rotation and resonance energy homotransfer, J. Microsc. 232/2 (2008) 306–312.
[33] G. Weber, Perrin revisited: Parametric theory of the motional depolarization of fluorescence, J. Phys. Chem. 93 (1989) 6069–6073.
[34] B. Corry, D. Jayatilaka, B. Martinac, P. Rigby, Determination of the orientational distribution and orientation factor for transfer between membrane-bound fluorophores using of a confocal microscope, Biophys. J. 91 (2006) 1032–1045.
[35] V. Ivanov, M. Li, K. Mizuuchi, Impact of emission anisotropy on fluorescence spectroscopy and FRET distance measurements, Biophys. J. 97 (2009) 922–929.
[36] F.M. Terhorst, P. Parham, D.L. Mann, J.L. Strominger, Structure of HLA antigens: amino-acid and carbohydrate compositions and NH_2-terminal sequences of four antigen preparations, Proc. Natl. Acad. Sci. U. S. A. 73 (1976) 910–914.
[37] C.J. Barnstable, W.F. Bodmer, G. Brown, G. Galfré, C. Milstein, A.F. Williams, A. Ziegler, Production of monoclonal antibodies to group A erythrocytes, HLA and other human cell surface anigens — new tools for genetic analysis, Cell 14 (1978) 9–20.
[38] M. Tanabe, M. Sekimata, S. Ferrone, M. Takiguchi, Structural and functional analysis of monomorphic determinants recognized by monoclonal antibodies reacting with HLA class I alpha 3 domain, J. Immunol. 148 (1992) 3202–3209.
[39] E.G. Spack Jr., B. Packard, M.L. Wier, M. Edidin, Hydrophobic adsorption chromatography to reduce nonspecific staining by rhodamine-labeled antibodies, Anal. Biochem. 158 (1986) 233–237.
[40] S. De Petris, Immunoelectron microscopy and immunofluorescence in membrane biology, in: E.D. Korn (Ed.), Methods in Membrane Biology, vol 9, Plenum Press, New York 1978, pp. 1–201.
[41] J.R. Lakowicz, Fluorescence Anisotropy. Ch. 10. In: Principles of Fluorescence Spectroscopy, Kluwer Academic/Plenum Publishers, New York, 1999 291–318.
[42] B. Valeur, Fluorescence polarization. Emission anisotropy, Molecular Fluorescence. Principles And Applications, Wiley-VCH, Weinheim 2002, pp. 125–154.
[43] T.M. Jovin, Fluorescence polarization and energy transfer: theory and application, in: M. Melamed, P. Mullaney, M. Mendelsohn (Eds.), Flow Cytometry and Sorting, J. Wiley & Sons, New York 1979, pp. 137–165.
[44] G. Szentesi, G. Horváth, I. Bori, G. Vámosi, J. Szöllősi, R. Gáspár, S. Damjanovich, A. Jenei, L. Mátyus, Computer program for determining fluorescence energy transfer efficiency from flow cytometric data on a cell-by-cell basis, Comput. Methods Prog. Biomed. 75 (2004) 201–211.
[45] H. Goldstein, C. Poole, J. Safko, The kinematics of rigid body motion. Ch. 4, Classical Mechanics, 3rd edditionAddison Wesley 2000, pp. 134–183.
[46] B.W. van der Meer, R.P. van Hoeven, W.J. van Blitterswijk, Steady-state fluorescence polarization data in membranes. Resolution into physical parameters by an extended Perrin equation for restricted rotation of fluorophores, Biochim. Biophys. Acta 854 (1986) 38–44.
[47] Q.S. Hanley, V. Subramaniam, D.J. Arndt-Jovin, T.M. Jovin, Fluorescence lifetime imaging: multi-point calibration, minimum resolvable differences, and artifact suppression, Cytometry 43 (2001) 248–260.
[48] L. Bene, T. Ungvári, R. Fedor, Sasi-Szabó László, L. Damjanovich, Intensity correlation-based calibration of FRET, Biophys. J. 105 (2013) 1–13.
[49] P. Nagy, G. Vámosi, A. Bodnár, S.J. Lockett, J. Szöllősi, Intensity-based energy transfer measurements in digital imaging microscopy, Eur. Biophys. J. 27 (1998) 377–389.
[50] G.H. Cross, A.A. Reeves, S. Brand, J.F. Popplewell, L.L. Peel, M.J. Swann, N.J. Freeman, A new quantitative optical biosensor for protein characterization, Biosens. Bioelectron. 19 (2003) 383–390.
[51] T. Heimburg, A.D. Jackson, On soliton propagation in biomembranes and nerves, Proc. Natl. Acad. Sci. U. S. A. 102 (28) (2005) 9790–9795.
[52] R. Hanbury Brown, R.Q. Twiss, Correlation between photons in two coherent beams of light, Nature 177 (1956) 27–29.
[53] M. Margittai, J. Widengren, E. Schweinberger, G.F. Schröder, S. Felekyan, E. Haustein, M. König, D. Fasshauer, H. Grubmüller, R. Jahn, C.A.M. Seidel, Single-molecule fluorescence resonance energy transfer reveals a dynamic equilibrium between closed and open conformations of syntaxin 1, PNAS 100 (26) (2003) 15516–15521.
[54] D. Canet, K. Doering, C.M. Dobson, Y. Dupont, High-sensitivity fluorescence anisotropy detection of protein-folding events: application to α-Lactalbumin, Biophys. J. 80 (2001) 1996–2003.
[55] L. Bene, G. Szentesi, L. Mátyus, R. Gáspár Jr., S. Damjanovich, Nanoparticle energy transfer on the cell surface, J. Mol. Recognit. 18 (2005) 1–18.
[56] G. Grynberg, A. Aspect, C. Fabre, Selection rules for electric dipole transitions. Applications to resonance fluorescence and optical pumping. Complement 2B *in*: introduction to quantum optics, From the semi-classical approach to quantized light, Cambridge University Press, Cambridge 2010, pp. 120–139.
[57] M. Nieto-Vesperinas, Optical theorem for the conservation of electromagnetic helicity: Significance for molecular energy transfer and enantiomeric discrimination by circular dichroism, Phys. Rev. A 92 (2015) (023813(1–8)).
[58] K.Y. Bliokh, F.J. Rodríguez-Fortuño, F. Nori, A.V. Zayats, Spin–orbit interactions of light, Nat. Photonics 9 (2015) 796–808, http://dx.doi.org/10.1038/nphoton.2010.201.
[59] D.L. Andrews, On the conveyance of angular momentum in electronic energy transfer, Phys. Chem. Chem. Phys. 12 (2010) 7409–7417.
[60] L. Bene, P. Gogolák, T. Ungvári, M. Bagdány, I. Nagy, L. Damjanovich, Depolarized FRET (depolFRET) on the cell surface: FRET control by photoselection, BBA MCR 1863 (2016) 322–334.
[61] D.S. Kliger, J.W. Lewis, C.E. Randall, Introduction to the Jones calculus, Müller calculus, and Poincaré sphere. Ch. 4, Polarized light in optics and spectroscopy, Academic Press Inc, Boston 1990, pp. 59–101.
[62] G. Steinbach, I. Pomozi, O. Zsiros, A. Páy, G.V. Horváth, G. Garab, Imaging fluorescence detected linear dichroism of plant cell walls in laser scanning confocal microscope, Cytometry A 73A (2008) 202–208.

Please cite this article as: T. Ungvári, et al., Perrin and Förster unified: Dual-laser triple-polarization FRET (3polFRET) for interactions at the Förster-distance and beyond, Biochim. Biophys. Acta (2016), http://dx.doi.org/10.1016/j.bbamcr.2016.02.002